Electronic surface resonances of crystals

E. G. McRae

Bell Laboratories, Murray Hill, New Jersey 07974

Electrons incident on a crystal surface can be temporarily trapped in surface states at energies above the vacuum level. These temporary or nonstationary surface states are observed as narrow fluctuations of elastic scattering intensity with respect to variation of electron energy and incidence direction. The scattering process is called electronic surface resonance scattering. The temporary surface states that are intermediate states in resonance scattering are called electronic surface resonances. The article surveys both experimental and theoretical research on electronic surface resonances as observed by scattering of low-energy (<1 keV) electrons. A critical account of experiments on Al(001), W(001), Ni(001), and oxygenated Ni(001) surfaces is offered together with theoretical commentary. Plots of the electronic surface resonance band structure $E(k_{\|})$ (E = resonance energy, $k_{\|}$ = reduced surface-parallel momentum) are compiled and the signficance of $E(k_{\|})$ plots for surface characterization is indicated.

CONTENTS

I. OBJECTIVES AND SCOPE

Electrons incident on a crystal surface can be temporarily trapped in surface states at energies above the vacuum level. These temporary or nonstationary surface states are observed as narrow fluctuations of elastic scattering intensity with respect to variation of electron energy and incidence direction. The scattering process is called electronic surface resonance scattering. The temporary surface states that are intermediate states in resonance scattering are called electronic surface resonances. Other terms in common use include electronic bound-state resonance, surface-state resonance, surface wave resonance and surface barrier resonance. All of these have exactly the same meaning as electronic surface resonance. Generally the term surface resonance is applied to any nonstationary surface state, but in the present article it is applied exclusively to temporary but long-lived surface states that exist at energies above the vacuum level in the absence of externally applied fields. The objectives of this article are to survey observations of electronic surface resonances and to indicate their significance for characterizing crystal surfaces.

The chief objective in the study of these and other surface states is to determine the dispersion of surface-state energies with respect to the surface parallel momentum—the electronic surface band structure—and to correlate the surface band structure with surface properties such as the geometrical or electronic structure of surfaces. The particular advantage of studying surface resonances is that, unlike surface states below the vacuum level, resonances are accessible to direct observation in elastic scattering experiments. In the elastic scattering of electrons at crystal surfaces both the energy and the surface-parallel momentum are con-

served quantities. Therefore the surface resonance band structure may be determined by mapping the positions of resonance fluctuations observed in any electron scattering experiment in which both the electron energy and momentum are resolved.

The earliest observations of electronic surface resonances were made in the course of pioneering high-energy (>10 keV) electron scattering experiments dating back to the 1930s. Since about 1960, however, almost all observations of electronic surface resonances have been made using low-energy (<1 keV) electron scattering methods. Only these low-energy electronic resonances are covered fully in the present article. A few references to high-energy electronic resonances and to analogous resonances in atom scattering are included but these are intended for historical perspective only. The coverage of low-energy electronic surface resonances is complete through 1978.

The present article is the first to offer an extended survey of low-energy electronic surface resonances. Miyake and Hayakawa (1970) reviewed resonances as observed in high-energy electron diffraction, and they pointed out that basically similar descriptions should apply at low energies as well. Other previous coverage of low-energy electronic surface resonances has been limited to brief outlines in publications on low-energy electron diffraction (Estrup and McRae, 1971; Pendry, 1974).

Background information on the interaction of low-energy electrons with solid surfaces and on the surface crystallographic nomenclature used in the present article may be found in a review by McRae and Hagstrum (1976). To save repeated references on the part of readers not familiar with these topics, the essential pieces of background are set out as follows:

Surface purity and surface order are paramount concerns in all experiments on crystal surfaces. Consequently, as a matter of routine, all experiments are done in ultrahigh vacuum, surfaces are prepared in vacuum by special methods (e.g., cleavage, sputtering, chemical reactions) and surface condition is monitored (e.g., Auger electron spectroscopy for purity, low-energy electron diffraction for order).

Terminology of diffraction: "Net," "reciprocal net," and "unit mesh" are 2-D (two-dimensional) analogs of "lattice," "reciprocal lattice," and "unit cell," respectively. A "beam" is a plane wave incident on a crystal surface or a plane wave reflected from a crystal surface as a result of elastic scattering (diffraction) of an incident wave. In the elastic scattering of electrons at crystal surfaces, the projection of electron momentum parallel to the surface is conserved mod2πg where g is a reciprocal-net vector. A diffracted beam resulting from parallel-momentum transfer 2πg is conventionally indexed by the components of g referred to the basic vectors of the reciprocal net of the substrate crystal. For example, if $\mathbf{g} = 2\mathbf{a}_1^* - 1\mathbf{a}_2^*$, where $\mathbf{a}_1^*$, and $\mathbf{a}_2^*$ are basic vectors of the reciprocal net, the beam is indexed $(2\bar{1})$. The net axes are designated by a crystallographic convention (Wood, 1964) indicated in Fig. 1. Throughout this article, notations of quoted authors are changed where necessary to conform to the convention.

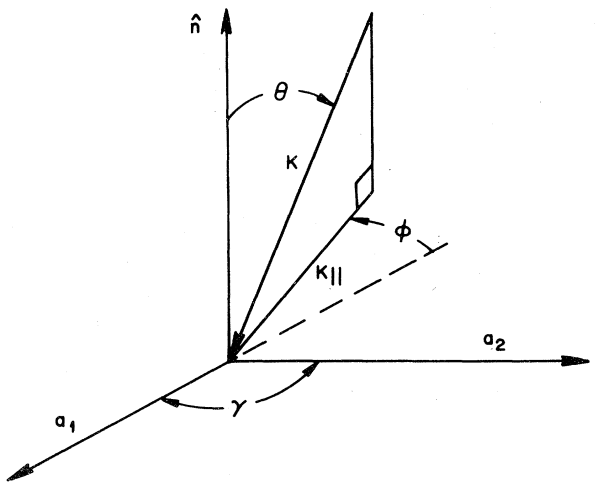

FIG. 1. Definition of angle variables θ and ϕ for incident particles and conventional designation of net axes. **K** denotes the total momentum, $\mathbf{K}_{\parallel}$ the surface-parallel momentum, $\hat{\mathbf{n}}$ the unit outward surface normal, $\mathbf{a}_1$ and $\mathbf{a}_2$ the basic vectors of the net, and γ the angle (in general obtuse) between $\mathbf{a}_1$ and $\mathbf{a}_2$.

Designation of crystal surfaces: If the unit mesh of a crystal surface has sides $(\mathbf{b}_1, \mathbf{b}_2)$ and is rotated by an angle $\alpha \neq 0$ with respect to the unit mesh $(\mathbf{a}_1, \mathbf{a}_2)$ of the ideal substrate surface, the surface periodicity is designated by $[(b_1/a_1) \times (b_2/a_2)]\alpha$. If $\alpha = 0$ the angle designation is omitted. Usually $c(2\times2)$—"centered" (2×2)—is used instead of $(\sqrt{2}\times\sqrt{2})45°$ and $p(2\times2)$—"primitive" (2×2)—is used instead of (2×2). Crystal surfaces are designated by shorthand such as Ni(001)$c(2\times2)$O [Ni substrate crystal, (001) substrate net plane, $c(2\times2)$ surface periodicity, O atoms adsorbed on the surface]. For atomically clean surfaces the designation (1×1) is usually omitted so that, e.g., Ni(001) means Ni(001)(1×1).

The material of this article is arranged as follows. Section II deals with the observation and identification of resonances. It consists of a schematic description of resonances and resonance scattering (Sec. II.A) followed by a chronological account tracing the introduction of various experimental methods (Sec. II.B). Section III deals with theory aimed at the description of the surface resonance band structure and of the width and lineshape of resonances as observed in low-energy electron scattering experiments. The topics treated are the general properties of resonances approached from the viewpoint of the analytic structure of the scattering amplitude and the relationship between reflection and emission intensities (Sec. III.A), general theoretical approaches including the two-dimensional nearly-free-electron description (Sec. III.B) and the layer multiple-scattering description (Sec. III.C), and a survey of applications of theory, including such special applications as temperature effects and spin polarization (Sec. III.D). Section IV offers a critical summary of experimental results available to date together with theoretical commentary. The material is arranged by crystal substrates comprising Al(001), W(001), and Ni(001) (Secs.

IV.A–C). The article ends with a survey of prospects for surface characterization by resonance experiments (Sec. IV.D).

II. INTRODUCTORY SURVEY

A. Nature of electronic surface resonances

An electron in a surface resonance has total kinetic energy above the vacuum level, but the part of its energy associated with the normal component of momemtum is below the vacuum level. Therefore the electron is prevented from escaping into vacuum by the surface potential barrier.

1. Limiting cases

Electronic surface resonances may be described approximately by either of two theoretical pictures that represent limiting cases of real situations. These cases correspond respectively to strong and weak overlap between the resonance electron density and the bulk scattering potential of the crystal.

The strong overlap (SO) picture is similar to the model customarily used for ordinary surface states at energies near or below the Fermi level. A SO resonance differs from an ordinary surface state only in having a large group velocity parallel to the surface. The SO resonance electron density is centered in the region occupied by the first few atom layers of the crystal. Like the band structure for ordinary surface states, the SO surface resonance band structure depends mainly on the effective potential near the atoms. It does not depend strongly on the long-range image potential outside the outermost atom layer. The SO resonance samples the bulk electron density of the crystal, so that the resonance intensity fluctuations are lifetime broadened by electron–electron interactions to the same extent as intensity features due to bulk scattering, e.g., Bragg peaks. The extent of the broadening is roughly equal to twice the imaginary (absorptive) part of the bulk optical potential. For most solids, measured values of the inelastic mean free path of low-energy electrons translate to absorptive-potential values of about 3 eV for electron energies above 50 eV. For decreasing electron energies the absorptive potential decreases to about 1 eV at energies near the vacuum level.

The weak overlap (WO) picture resembles the models used to describe the surface states of particles trapped in their image potential well, e.g., electrons at liquid He surface (Cole, 1974). The WO resonance electron density is centered outside the outermost atom layer of the crystal. The WO surface resonance band structure depends strongly on the long-range part of the potential, while the laterally periodic potential variation due to the shorter-range effects of surface atoms has a secondary role only. The appropriate starting point for a description of the surface resonance band structure in the WO case is that in which the electron motion in the two dimensions parallel to the surface is free. This is called the 2-D free-electron picture. WO resonances sample an electron density much smaller than that of the bulk crystal, so in that case the lifetime broadening of resonance intensity fluctuations is much smaller than that of bulk-scattering intensity features.

Experimentally, resonance intensity fluctuations may be identified as such on the basis of their width in energy. All observed elastic-scattering features less than about 1.5 eV wide can be assigned to resonances. This criterion admits only resonances conforming approximately to the WO picture. All observed features that have been assigned to resonances exhibit 2-D free-electron-like dispersion, as is consistent with the WO picture. Resonances conforming to the SO picture have been predicted but in electron scattering experiments they would be difficult to disentangle from bulk scattering features.

2. Two-dimensional free-electron description

The more important regularities and nomenclature of electronic surface resonances may be conveniently introduced in the framework of the 2-D free-electron description. It is obtained by replacing the scattering potential $U(z, \mathbf{r})$ of the crystal by a potential that retains the 2-D periodicity of the surface while approaching indefinitely closely to the laterally averaged potential $U_0(z)$ defined by

$$U_0(z) = A^{-1} \int U(z, \mathbf{r})\, d\mathbf{r}\,. \tag{1}$$

Here z denotes the inward surface normal coordinate, $\mathbf{r}$ denotes a position vector in the plane of the surface,

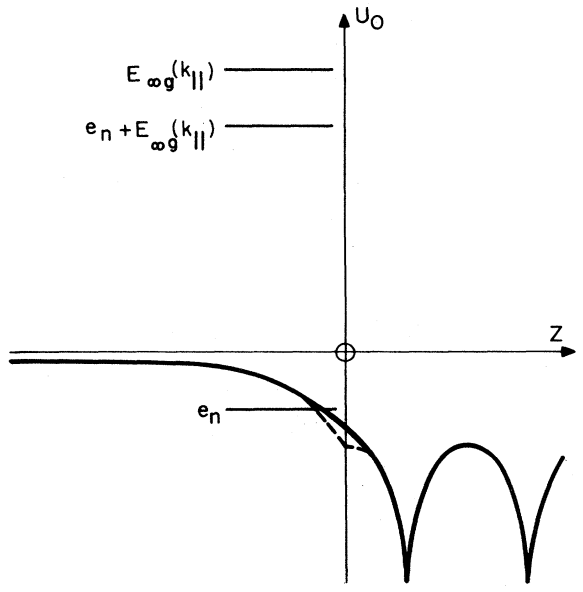

FIG. 2. Laterally averaged potential $U_0(z)$ for a crystal, together with energy levels pertaining to resonances according to the 2-D free-electron description (schematic). z is the inward surface-normal coordinate. $E_{\infty g}$ ($\mathbf{k}_{\parallel}$) denotes the threshold energy for the diffraction beam indexed by reciprocal-net vector $\mathbf{g}$, e_n denotes the nth bound-state energy eigenvalue for potential $U_0(z)$ and $e_n + E_{\infty g}$ ($\mathbf{k}_{\parallel}$) denotes the resonance energy. $\mathbf{k}_{\parallel}$ is the reduced parallel momentum. Broken lines indicate an idealized form of potential adopted for an approximate calculation of the eigenvalues e_n (text, Sec. III.C).

the integration is over one unit mesh of the surface, and A denotes the unit-mesh area. A possible shape of the laterally averaged potential $U_0(z)$ is sketched in Fig. 2.

In general the laterally averaged potential $U_0(z)$ supports bound surface states with wave functions

$$|ng\rangle = \psi_n(z) \exp[i(\mathbf{k}_{\parallel} + 2\pi\mathbf{g}) \cdot \mathbf{r}] \quad n = 1, 2 \ldots . \tag{2}$$

Here $\psi_n(z)$ denotes the nth surface-state solution (i.e., a solution vanishing for $|z| \to \infty$) of the Schrödinger equation for the potential $U_0(z)$. The existence of such solutions is well known (Jones, 1975). It depends on "forbidden gaps" in the band structure derived from $U_0(z)$. The forbidden gaps, together with the surface potential barrier, have the effect of confining electrons in the surface region of the crystal. The second factor of the wave function in Eq. (2) represents free-electron motion parallel to the surface. Here g denotes a vector of the reciprocal net of the surface and $\mathbf{k}_{\parallel}$ denotes the reduced parallel momentum—i.e., the momentum in the plane parallel to the crystal surface, mod2πg. The total parallel momentum is $\mathbf{k}_{\parallel} + 2\pi\mathbf{g}$.

The electron energies corresponding to the 2-D free-electron wave functions of Eq. (2) are

$$E_{ng}(\mathbf{k}_{\parallel}) = e_n + E_{\infty g}(\mathbf{k}_{\parallel}), \tag{3}$$

where e_n denotes the energy eigenvalue corresponding to ψ_n in Eq. (2), and the second term in Eq. (3) has the expression

$$E_{\infty g}(\mathbf{k}_{\parallel}) = \tfrac{1}{2}|\mathbf{k}_{\parallel} + 2\pi\mathbf{g}|^2 . \tag{4}$$

Here and in all equations in this article, Hartree atomic units ($\hbar = m = e = 1$) are used and all energy values are referred to the vacuum level as origin. $E_{\infty g}(\mathbf{k}_{\parallel})$ is the threshold energy (grazing emergence energy) for the diffracted beam indexed by reciprocal-net vector g. The energy-level separation $E_{\infty g} - E_{ng} = -e_n$ means the binding energy of the nth surface state associated with a given threshold, relative to the threshold.

The pattern of energy levels represented by Eq. (3) is sketched in Fig. 2. It is often convenient to think of the energy levels as consisting of sequences of levels where each sequence converges on its corresponding threshold level. Figure 2 shows one threshold level and one member of sequence converging on it.

The dispersion $E(\mathbf{k}_{\parallel})$ of surface-state energies E is called the surface band structure. The beam threshold functions $E_{\infty g}(\mathbf{k}_{\parallel})$ for different g values collectively make up the surface band structure in the free-electron limit $U(z, \mathbf{r}) \to 0$. In the 2-D free-electron description, the surface band structure for a given level index n is displaced to lower energies from the free-electron limit by a fixed amount equal to the binding energy $-e_n$.

The orders of magnitude of the quantities appearing in the 2-D free-electron description of low-energy electronic resonances may be appreciated from the examples given in this article, especially in Sec. IV. Typical values of the binding energy of an $n = 1$ level lie in the range 0.5–3 eV.

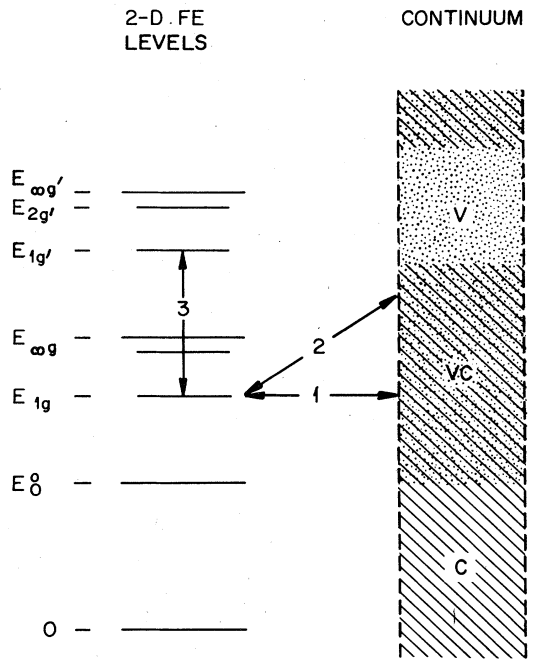

FIG. 3. Classification of perturbations of 2-D free-electron (FE) levels. Double-headed arrows connect interacting levels in each type of perturbation (see text, Sec. II.A). All levels have the same value of reduced parallel momentum and the same point symmetry. The subscripts 0, g, and g' label the beam thresholds in accordance with notation introduced in the text. Some representative energy values referred to the vacuum level as origin are indicated at the left. Shading indicates types of continuum state according to regions of electron propagation: V—propagation in vacuum only (forbidden gap); C—crystal only; VC—both vacuum and crystal.

3. Classification of perturbations of 2-D free-electron states

The 2-D free-electron description gives a picture of discrete surface states whose dispersion mimics that of the beam threshold conditions. This picture is modified by inclusion of the lateral variation of the potential. If the lateral variation of the potential is viewed as a perturbation, there are modifications arising from interactions between zeroth-order states with the same $\mathbf{k}_{\parallel}$ value and the same point symmetry. The possible kinds of interaction are indicated schematically in Fig. 3 and may be classified as follows: (1) resonance interactions between surface states and a continuum of states of electron propagation; (2) nonresonance interactions between surface states and a continuum; and (3) interactions between different surface states.

Each continuum state has the form of a superposition of plane waves in vacuum and a superposition of Bloch waves in the crystal. These plane waves and Bloch waves comprise both propagating waves and nonpropagating or evanescent waves. For each $\mathbf{k}_{\parallel}$ value there are some energy ranges in which electron propagation is confined either to vacuum or to the bulk crystal. For energies less than $E_{\infty 0}(\mathbf{k}_{\parallel}) = \frac{1}{2}\kappa_{\parallel}^2$ there are no propagating plane waves. For energies lying in the range of a forbidden gap in the 3-D band structure of the crystal there

are no propagating Bloch waves. The term "forbidden gap" refers to the 1-D section through the band structure fixed by the value of $k_{\parallel}$. There may of course be some energy ranges that are not strictly forbidden gaps but within which the interactions with states of propagation in the crystal are weak; these "partially forbidden" gaps have qualitatively the same significance as forbidden ones.

Resonance interactions (interactions of type 1, Fig. 3) are the basis of elastic-scattering methods of investigating electronic surface states. Resonance interactions provide first the mechanism whereby surface states can be populated by elastic transitions from propagating states, and second they provide a mechanism of decay of surface states to propagating states with attendant broadening of surface levels. Narrow resonances are expected only in the energy ranges of forbidden or partially forbidden gaps. Inside a forbidden gap, resonances can decay only to states propagating in vacuum. Outside any such gap, but above the threshold $E_{\infty 0}(k_{\parallel})$, resonances can decay to continuum states that are propagating both in the crystal and in vacuum.

The other interactions represented in Fig. 3 cause shifts of 2-D free-electron levels. In particular the surface state–surface state interactions (type 3, Fig. 3) depend critically on the geometric and electronic structure of the surface. The resulting pattern of levels is characteristic of the crystal surface in question.

4. Mechanism of resonance scattering

Resonance scattering of electrons at crystal surfaces is a special case of a general phenomenon having an important part in several branches of physics such as nuclear physics and atomic physics (Newton, 1966). In the most general sense of the term, resonance scattering denotes the capture of an incident particle by the target to form a compound state which subsequently decays to release the scattering products. A given compound state can generally decay by several paths or "channels" which are characterized individually by the final quantum states of the target and of the scattered particles. Resonance scattering occurs with appreciable probability only in a narrow range of incidence energy and momentum characteristic of the compound state. It always occurs at the same time as "direct" or nonresonance scattering, whose probability varies relatively slowly with respect to the incidence conditions. The coherent superposition of the resonance and direct contributions to the scattering amplitude results in a fluctuation of scattering intensity centered at values of incidence energy and momentum for which the magnitude of the resonance contribution is at a maximum. The width in energy Γ of the fluctuation is related inversely to the lifetime Δt of the compound state through the relation $\Gamma \Delta t \approx \hbar$.

Each of the general properties of resonance scattering has a particular realization in scattering at crystal surfaces. In surface resonance scattering the intermediate compound state is a surface state. In an electron scattering experiment, a resonance is observed as a fluctuation of scattering intensity centered at values of incidence electron energy E and reduced parallel momentum $k_{\parallel}$ characteristic of the surface state.

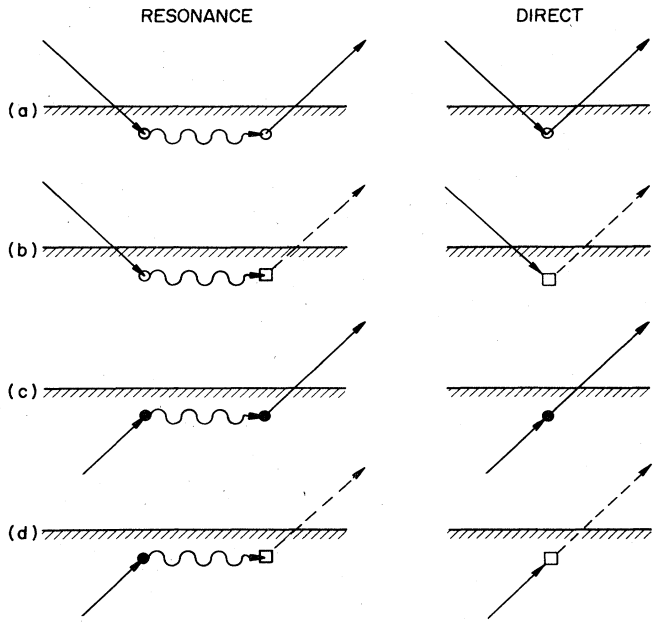

FIG. 4. Resonance and direct mechanisms of electron scattering at a crystal surface: (a) elastic reflection, (b) inelastic reflection, (c) elastic emission, and (d) inelastic emission. Straight arrows denote incident or elastically scattered electron waves, wavy arrows denote surface states, broken arrows denote inelastically scattered electron waves, open circles denote elastic scattering with change of surface-parallel momentum, filled circles denote elastic scattering with or without change of surface-parallel momentum, and open squares denote inelastic scattering.

The mechanism underlying such observations in indicated schematically in Fig. 4. The intermediate surface state may be excited by an electron incident from vacuum [reflection case, Fig. 4(a), (b)] or from the bulk crystal [emission case, Fig. 4(c), (d)]. The surface state may decay by an elastic channel [Fig. 4(a), (c)] or an inelastic one [Fig. 4(b), (d)]. Resonances may be observed in either elastic or inelastic scattering experiments, depending on the decay channel monitored.

The $(E, k_{\parallel})$ values derived from observation of a narrow resonance intensity fluctuation are independent of the scattering mechanism responsible for it. However, the line shape of the fluctuation depends critically on the mechanism. This is so because the scattering amplitude is the superposition of two contributions, namely the resonance and direct contributions as indicated schematically for each process in Fig. 4. The line shape is the sum of the squared modulus of the resonance amplitude contribution and the cross-term due to the interference between the resonance and direct terms. There are important limiting cases depending on the ratio of the magnitude of the resonance amplitude contribution at its maximum to that of the direct contribution. In the limit of small resonance/direct ratios the line shape is due to the cross term only, so that it may be a peak, a dip, or an asymmetric feature depending on the phase of the superposition of resonance and direct contributions to the amplitude. In the

opposite limit, only the resonance term is present so that the fluctuation must be a symmetric peak.

B. Chronology of surface resonance observations

Surface resonance observations depend on the determination of the energy E and the parallel momentum $k_{\parallel}$ of particles incident on or emitted from a crystal surface. The experimental variables are the energy E, the colatitude angle of incidence or emission θ, and the azimuthal angle of incidence or emission ϕ. Definitions of the angle variables for incident particles are shown in Fig. 1. The corresponding definitions for emission are obtained by reversing the directions of the total momentum $\mathbf{K}$ and of the parallel momentum $\mathbf{K}_{\parallel}$.

1. Atom scattering

Surface resonances are known in the contexts of both atom scattering and electron scattering. There has been a parallel development in understanding of resonances in these two contexts. The first observations of surface resonances were made in the course of atom scattering experiments by Stern and his co-workers in the early 1930s. Their experiment on the reflection of He atoms by a LiF(001) surface (Esterman and Stern, 1930; Frisch and Stern, 1933) was the first to show diffraction of atoms by crystals. It also showed narrow minima in the intensity of specular reflection under incidence conditions near those for beam thresholds. These features were explained (Lennard-Jones and Devonshire, 1936; Devonshire, 1936) by a process in which an incident atom is temporarily captured in a surface state. Subsequent experiments have confirmed the role of surface states in atom scattering by resolving an expected pattern of several features converging on a single threshold. This kind of pattern was introduced in Sec. II.A with reference to electronic resonances but the same picture applied to atomic surface resonances as well. The early observations showed line shapes consisting exclusively of minima, leading Lennard-Jones and Devonshire to propose a resonance process with inelastic decay analogous to that of Fig. 4(b). They called this "selective adsorption." However, it is now known that a variety of line shapes are possible and that both types of resonance reflection process indicated in Fig. 4 can occur in atom scattering. Recent developments in atom scattering have been reviewed by Goodman (1977).

2. High-energy electron diffraction

The first observation of resonance scattering of electrons at crystal surfaces was made by Kikuchi and Nakagawa (1933). Their observation was made as part of a study of high-energy (40–100 keV) reflection electron diffraction at the (011) cleavage face of zinc blende crystal. They reported that the intensity at the Bragg peak of the specularly reflected beam is at a relatively very high maximum under conditions later recognized by Miyake, Kohra, and Takagi (1954) as being close to threshold conditions for diffracted beams. The effect was called an "intensity anomaly" by the original authors but is now more commonly referred to as "enhancement." The review by Miyake and Hayakawa (1970) traces the evolution of the interpretation of enhancement and contains photographs of diffraction patterns to illustrate that phenomenon.

The definitive interpretation of enhancement as a resonance-scattering effect was given by Kohra, Molière, Nakano, and Ariyama (1962). They recognized explicitly the role of a "surface wave" or surface-localized electronic state. The mechanism involved is that of Fig. 4(a). The appearance of a very high intensity maximum apparently means that the resonance/direct ratio is large. The interference between resonance and direct contributions is relatively unimportant, but some degree of interference is evidenced by asymmetric line shapes in some experiments.

While Kohra *et al.* were the first to deal theoretically with the enhancement phenomenon, the nature of electronic surface resonances at energies of the order of 50 keV was earlier treated by Artmann (1947) in connection with Kikuchi lines in the background to diffraction patterns.

Artmann's work dealt with anomalies in the vicinity of Kikuchi-line envelopes. These terms require some explanation. Kikuchi lines are due to electrons that have suffered inelastic scattering followed by multiple

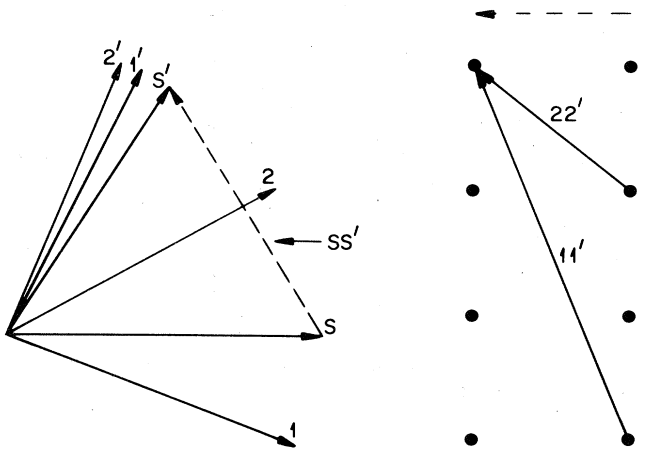

FIG. 5. Geometry of Kikuchi lines and envelopes of Kikuchi lines. The wave field due to inelastically scattered electrons in a crystal is imagined to be resolved into plane-wave components. The propagation vectors for three special components of the same energy are indicated at left by 1, 2, and S. Vectors 1, 2, and S lie in a common plane perpendicular to the surface. In this plane the reciprocal lattice has points indicated at the right. Vectors 1 and 2 are vectors for which Bragg reflection conditions are satisfied. Vector S is parallel to the surface. The initial vectors 1 and 2 are related by Bragg reflections to vectors 1′ and 2′ respectively. The momentum transfers are 2π times those indicated by arrows at right. The initial vector S is related to S' by the same surface component of momentum transfer, i.e., 2π times that indicated by the broken arrow at right. Projections of 1′ and 2′ on a viewing screen are points on Kikuchi lines. The projection of S' is a point on the envelope of all Kikuchi lines corresponding to the same surface component of momentum transfer. The complete Kikuchi lines are intersections with the viewing screen of cones having axes 11′, 22′. The complete envelope is the intersection with the cone having axis SS'.

elastic scattering in the course of their escape from the crystal. The dominant process of elastic scattering is Bragg reflection in the bulk crystal. The term Bragg reflection denotes conservation of momentum mod2π times a vector of the reciprocal lattice. Thus, for example, in Fig. 5 inelastically scattered waves that have the same energy and that travel in directions 1 and 2 give rise to Kikuchi lines in emission directions 1′ and 2′, respectively. In the azimuth represented in Fig. 5, the limiting direction of all the Kikuchi lines that can be obtained for a given surface component of momentum transfer in that azimuth is the direction S' corresponding to an initial direction S parallel to the surface. Generally, the emission directions such as S', corresponding to initial directions parallel to the surface such as S, form envelopes of Kikuchi lines. From Fig. 5 it is apparent that the emission directions for a Kikuchi-line envelope are related by reciprocity to the directions for the thresholds of diffracted beams. In other words, in the notation of Sec. II.A, the $(E,\mathbf{k}_{\parallel})$ values for a Kikuchi-line envelope satisfy a relation of the form $E = E_{\infty g}(\mathbf{k}_{\parallel})$.

Artmann showed that the mechanism responsible for intensity anomalies near the Kikuchi-line envelopes is emission by a resonance scattering process of the type represented in Fig. 4(c). He further described the intensity distribution near the envelope as a sequence of "surface" Kikuchi lines parallel to the envelope and converging on it. In the notation of Sec. II.A, the $(E,\mathbf{k}_{\parallel})$ values for this sequence of Kikuchi lines were found to satisfy an equation of the form $E = E_{ng}(\mathbf{k}_{\parallel})$, $n = 1, 2, \ldots$. Just as in electron reflection resonances form a sequence converging on each beam threshold, so in electron emission resonances form a sequence of surface Kikuchi lines converging on each envelope of bulk Kikuchi lines.

3. Low-energy electron diffraction (LEED)

The first observation of resonance elastic scattering of low-energy electrons was reported by McRae and Caldwell (1964). They made LEED observations using the experimental setup diagrammed in Fig. 6. They used the retarding field mode of operation in which the sample is biased negatively with respect to the first grid. The retarding field serves as an additional focusing control of the primary beam and it reduces distortions of the beam due to stray magnetic and electric fields. In the retarding mode, diffracted electrons traveling parallel to the crystal surface are pulled back to the fluorescent display screen as indicated in Fig. 6. Thus as the electron energy increases, the grazing emergence of new beams as well as the intensity variation of existing beams may be monitored. In observations on Li(001) surfaces, later extended to cleavage faces of NaF and graphite (McRae and Caldwell, 1967), resonance intensity minima were seen as dark lines traversing the (00) spot under the same conditions as for the grazing emergence of the (01) beam. Corresponding to this visual observation, plots of the (00) (specular) beam intensity versus electron energy were found to contain narrow minima (width < 2 eV) displaced by an amount of the order of 1 eV to the low-energy side of the beam thresholds. The displacements from the threshold were found to be insensitive to the incidence direction. A pair of experimental curves illustrating this regularity is reproduced in Fig. 7.

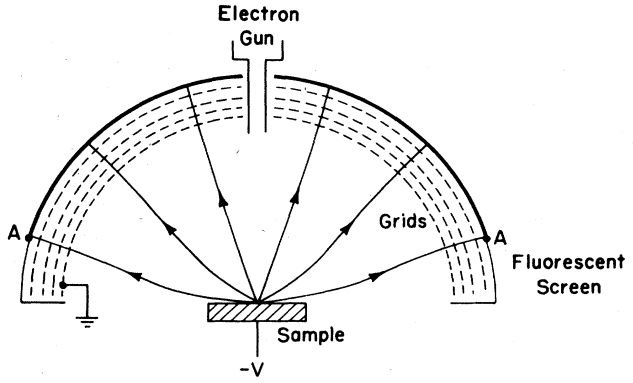

FIG. 6. Schematic cross section of conventional LEED apparatus indicating the retarding-potential mode of operation. The sample is biased negatively with respect to the first grid so that the focus of the incident beam is improved for low incidence energies. The diffraction pattern is contracted as indicated. Grazing emergence beams are pulled in to points A. Beam intensities are determined using a spot photometer to measure the brightness of diffraction spots. (Reproduced from Henrich, 1975).

Other LEED observations with qualitatively similar results were made on Cu(001) (Andersson 1970) and on other metal (001) surfaces (See. Sec. IV). A resonance associated with an adsorbate induced beam threshold

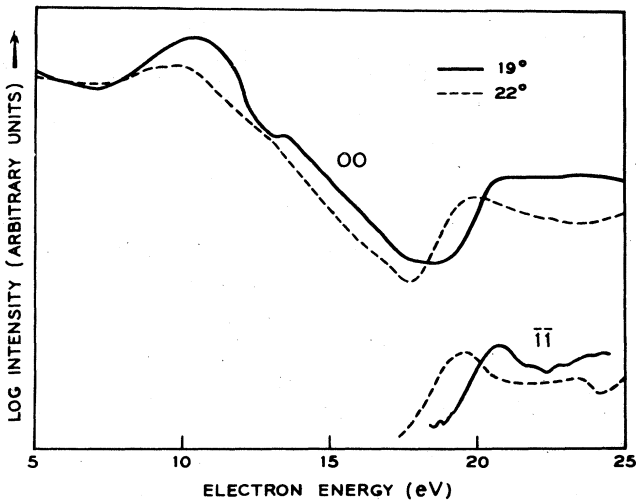

FIG. 7. LEED intensity curves for LiF (001). The measurements were made at the indicated colatitude angles of incidence in the [11] azimuth [crystallographic notations and beam indices refer to the LiF (001) net]. The resonance is observed as a (00) intensity minimum about 2 eV wide, centered near 18 eV. The $(\bar{1}\bar{1})$ beam threshold is marked by the rise of $(\bar{1}\bar{1})$ intensity near 19 eV (see Fig. 6 for the experimental method for grazing-emergence beams). The figure illustrates the correlation between the energies of the resonance feature and of the $\bar{1}\bar{1}$ threshold. (Reproduced from McRae and Caldwell, 1967).

was observed by LEED on W(001)$c(2\times2)$H (McRae and Wheatley, 1972).

The LEED observations can be accounted for by the mechanisms of Fig. 4(a) and (b). The role of an intermediate surface state was pointed out by Hirabayashi (1968) in a theoretical treatment patterned on that of Lennard-Jones and Devonshire for atom scattering.

In terms of the 2-D free-electron description of the intermediate surface state (Sec. II.A), the resonance structure observed by LEED may be assigned arbitrarily to the lowest-order ($n=1$) resonance for each threshold, and its displacement from the threshold may be identified with the binding energy $-e_1$. The assignment of the structure to $n=1$ rather than some larger integer is arbitrary as there is always the possibility of additional, lower-energy resonance structure too broad to identify as a resonance. Higher-order ($n>1$) resonances are predicted in general (Sec. II.A) but cannot be observed in conventional LEED experiments because of the limited energy resolution of those experiments (typically 0.5 eV). The cited experiments established that the resonance binding energy $-e_1$ is of the order of 1 eV.

The resonances observed in LEED are qualitatively the same as enhancement in high-energy electron diffraction (Miyake and Hayakawa, 1970). In LEED, however, the resonances apparently conform most often to the case of small resonance/direct ratios and a variety of resonance line shapes may be obtained. The gradual development from LEED resonances to enhancement with increasing electron energy up to a few keV was demonstrated in experiments on MgO(001) surface by Hayakawa and Miyake (1974).

Kikuchi lines due to low-energy resonances were first observed by De Bersuder (1968) in the course of LEED experiments on Al(001) surface. The experiments were done using a LEED goniometer (De Bersuder, 1974; Fig. 8) whose performance in resonance experiments has proved superior to that of the widely used LEED apparatus as shown in Fig. 6. De Bersuder noted that the quasielastic background to the LEED pattern contained special Kikuchi lines related to the two-dimensional periodicity of the surface. He called these Kikuchi lines K2 lines to distinguish them from ordinary Kikuchi lines (K3 lines) that arise from the three-dimensional periodicity of the bulk crystal and that are also present in the LEED background. A stereographic projection showing the geometry of the K2 lines (observed as dark lines) is reproduced in Fig. 9.

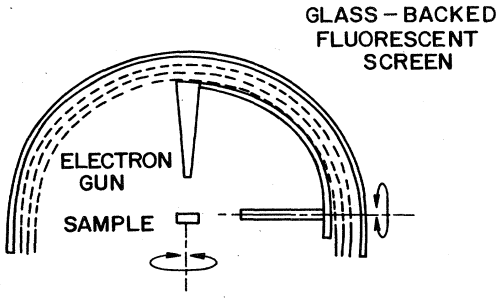

FIG. 8. Schematic cross section of a LEED goniometer. Beam intensities are determined using a traveling spot photometer mounted behind the glass backing of the fluorescent screen. (Adapted from De Bersuder, 1974).

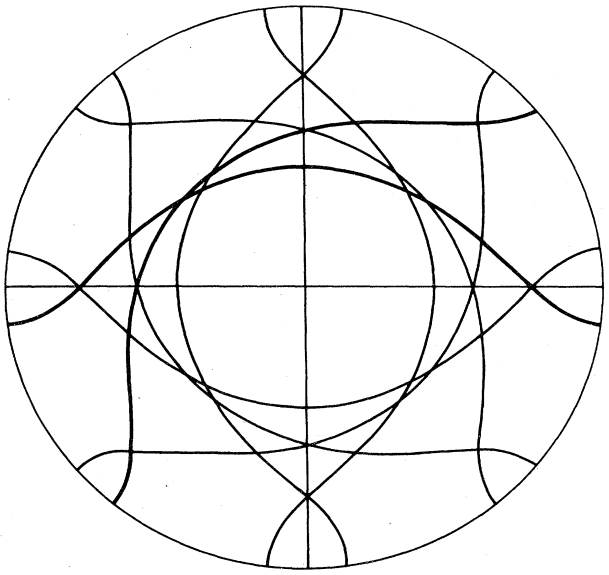

FIG. 9. Geometry of K2 lines observed for Al(001) surface. The center of the figure corresponds to the surface-normal direction. Two K2 lines are shown by thick lines for clarity. Electron energy 500 eV. (Adapted from De Bersuder, 1968).

The geometry of K2 lines may be summarized by the statement that the K2 lines correspond within experimental error to emission directions that are related by reciprocity to the incidence directions for the thresholds of diffracted beams. De Bersuder suggested that the mechanism responsible for K2 lines is a resonance scattering mechanism analogous to that responsible for LEED resonances. In line with that suggestion, McRae (1971) proposed the resonance emission mechanism represented in Fig. 4(c) of the present article.

The intimate connection between the K2 line and the resonance effect in LEED beam intensities was demonstrated by LEED experiments on Ni(001) (Andersson and Kasemo, 1971) in which the incidence conditions were varied to make the (00) spot cross a K2 dark line. As it crossed the K2 line, the spot was split symmetrically under the same conditions as those for a resonance minimum in the total spot intensity. Thus in LEED experiments as cited above, where the LEED spot is traversed by a resonance dark line, this dark line is geometrically the prolongation of a K2 line (possibly of very low contrast) in the background.

Apparently the K2 lines are completely analogous to the surface Kikuchi lines near the Kikuchi line envelopes as first treated in the high-energy case by Artmann. However, it has not been possible as yet to resolve structure due to individual members of the expected sequence of K2 lines converging on the envelope of K3 lines. Nor has it been possible to detect the displacement of K2 lines from the envelope of K3 lines.

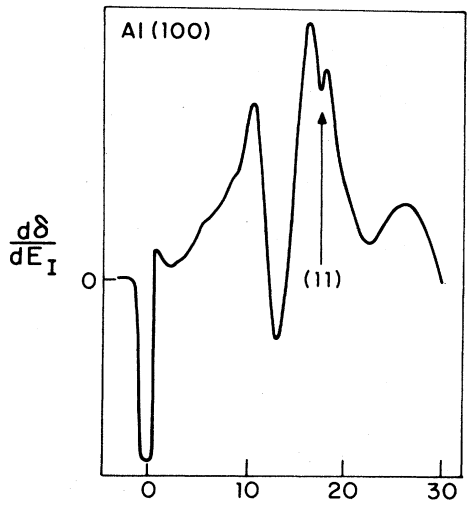

FIG. 10. Net-current plot for Al(001) surface, normal incidence. E_1 denotes the incidence electron energy. The quantity plotted is the derivative of the negative of the net current, which is proportional to the derivative of the secondary yield δ (see text, Sec. II.B). The arrow indicates the (11) beam threshold. The intensity fluctuation at almost the same energy as the threshold is interpreted as a resonance associated with that threshold. (Reproduced from Henrich, 1975).

4. Net-current low-energy electron reflection

A variant of the LEED method of observing resonances was introduced by Henrich (1975). It is called the net-current low-energy electron reflection method. The experimental setup is similar to that of conventional LEED (Fig. 6) but instead of measuring the reflection intensities in individual beams one measures the net current passing between the cathode of the electron gun and the crystal. To simplify the interpretation of the experiment, the conditions are chosen so that an electron reflected by the crystal has a negligibly small chance of returning to the crystal or to the mount in contact with it. Under these conditions the negative of the net current varies like the total reflection coefficient (secondary yield) with respect to variation of incidence energy or direction. It is assumed that the inelastic reflection coefficient is a slowly varying function of the incidence energy and direction, in which case the resonance fluctuations of the net current occur at the same $(E, \mathbf{k}_{\parallel})$ values as those in the total elastic reflection coefficient. In practice it is important to remove the background due to inelastic scattering and nonresonant elastic scattering so as to accentuate the relatively narrow resonance structure. In Henrich's experiment this was done by analog differentiation. An illustrative experimental curve obtained in the derivative mode is reproduced in Fig. 10.

The surface resonance band structure derived from the net-current low-energy electron reflection method is the same as that from LEED because all diffraction beams have resonances in common. However, different and relatively complex line shapes may be observed because they are in general the superpositions of line shapes from different LEED beams.

5. Secondary electron emission

Another experimental approach to electronic surface resonances is angle- and energy-resolved secondary electron emission. The most useful form of the method is that in which the direction of collection can be varied. This kind of technique was introduced first by Best (1975) and was used soon afterwards by Willis, Feuerbacher and Christensen (1977). The type of apparatus used by the latter authors and some representative experimental curves are shown in Figs. 11 and 12(a), respectively.

The observation of resonances by secondary electron emission is an extension of earlier work of Willis and co-workers in which that technique was used to determine the surface projection of the bulk density of states, including in particular the edges of forbidden gaps. The useful energy range of the technique extends from the vacuum level up to the bulk plasmon energy $\hbar\omega_p$; at energies above $\hbar\omega_p$ the structure is smeared out by electron-electron interactions. Figure 12(b) shows reduced secondary electron emission data of Willis *et al.* together with identifications of the features attributed to resonances and forbidden gaps. The assignment of specific features to resonances was based in this case on the correlation with the forbidden gap.

The mechanism underlying the observation of resonances in secondary electron emission is not well understood. One extreme possibility is that the contributions to the emitted wave field due respectively to the decay of bulk and surface states are relatively incoherent. This situation would obtain if the surface states were excited solely by direct electronic transitions from states below the Fermi level as has been assumed in the interpretation of some recent experiments (Best 1979a, b). In this "incoherent" case, the secondary emission spectrum would be a superposition of bulk and surface density-of-states contributions, each modified by slowly varying transition matrix factors. All resonances would be observed as symmetrical intensity peaks. The opposite extreme possibility is that bulk- and surface-state contributions to the wave field are relatively coherent and so can interfere with each other in the manner indicated by Fig. 4(c)

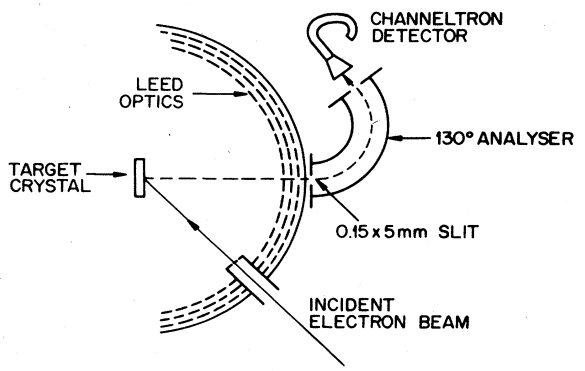

FIG. 11. Schematic cross section of apparatus used in measurements of angle and energy resolved secondary electron emission. (Reproduced from Willis, 1975).

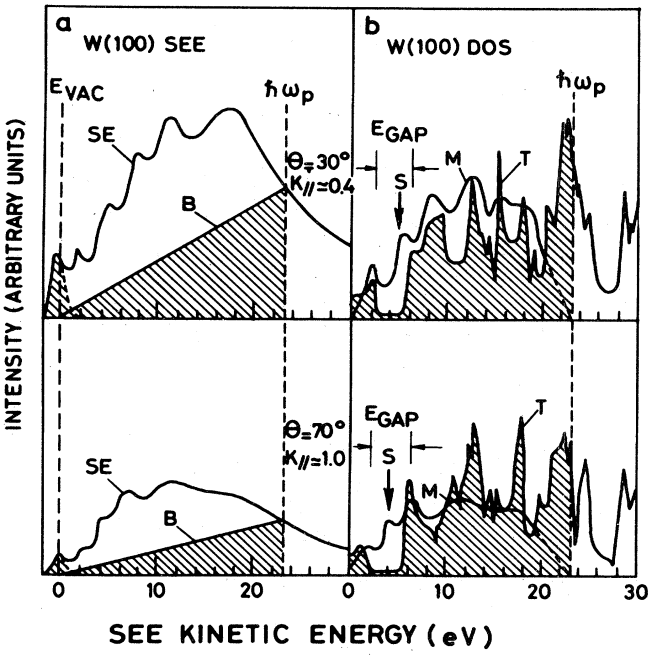

FIG. 12. (a) Angle- and energy-resolved secondary electron emission (SEE) spectra for W(001) surface. SE—intensity of secondary emission. B—background curve subtracted in the reduction of data. E_{vac} and $\hbar\omega_p$ denote the vacuum level and the bulk plasmon energy, respectively. The peak centered at E_{vac} was subtracted in the reduction of data. θ and $k_{||}$ denote the colatitude angle of emission and the reduced parallel momentum, respectively. (b) Reduced secondary electron emission data (M) compared with a theoretical plot of the bulk density of states (DOS). Vertical lines indicate the edges of the forbidden gap (width E_{gap}). S denotes the position of the resonance feature. [Adapted from Willis, Feuerbacher, and Christensen (1977)].

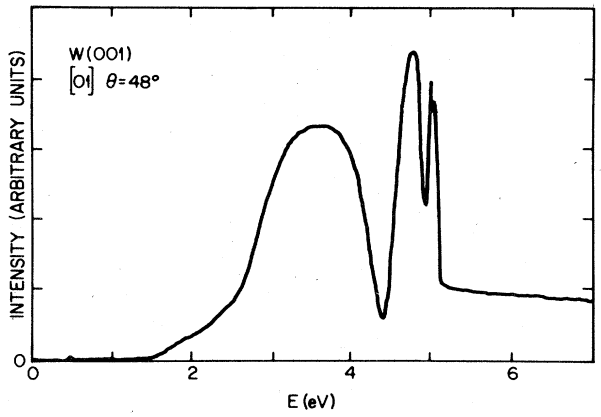

FIG. 13. LEED (00) beam intensity measured with high resolution as a function of incidence energy for W(001) surface. Colatitude angle of incidence 48°, incidence azimuth [01]. Three peaks, at 4.75, 4.97, and 5.03 eV, respectively, are identified as members of a sequence of resonances associated with the (01) beam threshold near 5.1 eV. (Adapted from Adnot and Carette, 1977a).

and (d). In this "coherent" case the secondary emission spectrum in the absence of surface states would still resemble the density-of-states plot, but resonances could appear with various line shapes depending on the phase of interference between resonance and direct contributions to the wave field. Theory for the coherent case (Sec. III.A) indicates that the $(E, \mathbf{k}_{||})$ dependence of secondary emission intensities resembles the $(E, -\mathbf{k}_{||})$ dependence of one minus the total elastic reflection coefficient.

6. High-resolution LEED

The electron scattering and electron emission experiments described above all lack the resolution required to detect fine structure due to the expected sequence of electronic surface resonances converging on each threshold. Only the lowest-energy ($n=1$) member of each sequence has been resolved in these experiments. However, Adnot and Carette (1977a) reported LEED measurements with a tandem of 127° electrostatic electron spectrometers capable of resolving higher-order structure. Results obtained for the W(001) surface (Fig. 13) clearly show the first three members of the resonance sequence converging on the (01) beam threshold near 5 eV (Adnot and Carette, 1977b). Similar results were reported subsequently by Willis (1978).

7. Photoemission

While elastic electron scattering is the simplest experimental approach to electronic surface resonances, it is also possible to observe resonances by spectroscopic methods—i.e., by the excitation of electronic transitions. This possibility was realized in photoemission experiments by Rowe, Margaritondo, and Christman (1977) as interpreted by Schlüter and Cohen (1978). The surfaces studies were clean, hydrogenated, and chlorinated Si(111)(2 × 1) surfaces obtained by cleavage.

The experiment was of the "constant initial state" type. In this type of experiment the photon energy $\hbar\omega$ is varied and the measured quantity is the flux of emitted electrons of kinetic energy $E=\hbar\omega-\Delta E$ where ΔE is fixed. The experiment yields a transition density function for initial states at an energy ΔE below the vacuum level. The observed structure in the transition density function was found to extend up to 15 eV above the vacuum level. The structure was assigned to electronic surface resonances on the basis of a comparison with computed transition densities. The computation involved separate determinations of the surface resonance band structure and of the relevant transition matrix elements. The band-structure computation did not take account of the long-range potential, so the results referred to resonances having "strong overlap" with the bulk crystal potential. The experimental results were not resolved with respect to emission direction, so the computational results were averaged to make the comparison with experiment as shown in Fig. 14.

Another type of photoemission technique—the partial photoyield technique—has also been used to detect resonances (Bachrach, Chadi and Bianconi, 1978). A peak

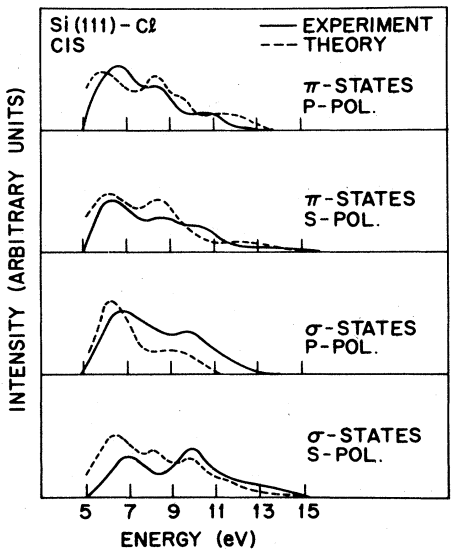

FIG. 14. Constant initial state (CIS) spectra for Si(111) with chemisorbed Cl. The experimental curves were obtained using synchrotron radiation at an incidence angle of 45° and polarized either parallel to the plane of incidence (*s* polarization) or perpendicular to it (*p* polarization). The value of ΔE (see text, Sec. II.B) was set to select either σ-type or π-type initial states localized at Cl atoms. The agreement between the theoretical and experimental curves confirms that the final-state effects are due to transitions to electronic surface resonances. (Reproduced from Schlüter and Cohen, 1978).

in the photoyield is observed for photon energies matching those of transitions from core levels to resonances. Transitions from the Al $L_{2,3}$ level to resonances were observed for Al(001) and Al(111) surfaces.

8. Other observations

Any electron reflection or election emission experiment ought to contain resonance structure. Other but as yet isolated examples are cited in connection with theory (Sec. III.D).

III. THEORY

A. General properties

1. Analysis of reflection amplitudes

Some of the general properties of resonances can be described with reference to the analytic structure of the scattering amplitude considered as a function of complex electron energy E. In this kind of description, all properties of physical significance are obtained in a limit of real energies such as

$$\mathrm{Im}\,E \to +0. \tag{5}$$

However, these physically significant properties are described with reference to singularities that are in general complex. The analysis is given in textbooks (Landau and Lifshitz, 1965) for scatterers of finite size. Some modifications of the textbook analysis are needed to treat electron scattering by a semi-infinite crystal (Gersten and McRae, 1972). The following is a condensed account of the analysis giving the main results bearing on surface resonances. Only the reflection case is treated. The relation between reflection and emission intensities is treated subsequently (Sec. III.A.*2*).

The important properties of reflection amplitudes may be obtained by considering an incident plane wave and any two elastically reflected wave. Other reflected waves will always be present, but they play no part in the present discussion.

Imagine that the electron wave field in vacuum consists of an incident plane wave with energy E and surface-parallel momentum $\mathbf{k}_{\parallel}$ and two elastically reflected waves with surface-parallel momenta $\mathbf{k}_{\parallel}$ and $\mathbf{k}_{\parallel}+2\pi\mathbf{g}$, respectively, where $\mathbf{g}$ is a reciprocal net vector. Along the surface normal passing through the origin of coordinates, the wave field has the expression

$$a(E,k_\perp^{(0)})(k_\perp^{(0)})^{-1/2}\exp(ik_\perp^{(0)}z)+a(E,-k_\perp^{(0)})(k_\perp^{(0)})^{-1/2} \times\exp(-ik_\perp^{(0)}z)+a(E,-k_\perp^{(g)})(k_\perp^{(g)})^{-1/2}\exp(-ik_\perp^{(g)}z), \tag{6}$$

where z is the inward surface-normal coordinate, the a's are plane-wave coefficients (independent of z) and $k_\perp^{(0)}, k_\perp^{(g)}$ denote surface-normal momentum components. The plane waves are normalized to the same surface-normal current density. In terms of the beam threshold energies $E_{\infty 0}$ and $E_{\infty g}$ introduced in Sec. II.A, the normal momentum components have the expressions

$$k_\perp^{(0)}=(2E-2E_{\infty 0})^{1/2}, \tag{7}$$

$$k_\perp^{(g)}=(2E-2E_{\infty g})^{1/2}. \tag{8}$$

Hartree atomic units ($\hbar=m=e=1$) are used.

The above expression for the wave field, Eq. (6), does not suffice to define the reflection amplitude. Additional specifications of the real and imaginary parts of the surface-normal momentum components are needed: (i) to identify the incident and reflected waves as such, and (ii) to specify the boundary condition satisfied by the reflected wave field in the limit $z\to-\infty$. Particular specifications are

$$\text{(i)}\ \mathrm{Re}\,k_\perp^{(0)}>0,\ \mathrm{Re}\,k_\perp^{(g)}>0, \tag{9}$$

$$\text{(ii)}\ \mathrm{Im}\,k_\perp^{(0)}>0,\ \mathrm{Im}\,k_\perp^{(g)}>0. \tag{10}$$

The first of these specifications (often referred to as the "outgoing wave" condition) identifies the first term in the expression for the wave field, Eq. (6), as the incident wave and the other two terms as reflected waves. Consequently the ratio of coefficients

$$T(E)=a(E,-k_\perp^{(0)})/a(E,k_\perp^{(0)}) \tag{11}$$

is an amplitude reflection coefficient. The second specification, Eq. (10), is equivalent to the physically acceptable boundary condition that the reflected wave field vanish in the limit $z\to-\infty$. It corresponds to one sheet, called the "physical sheet," of the many-valued function $T(E)$ (Fig. 15).

The amplitude reflection coefficient $T(E)$ is required on physical grounds to satisfy the additional physical requirement of causality. It means that $T(E)$ must be analytic over the upper half-plane of the physical sheet.

The following discussion deals with representative singular points of the reflection amplitude coefficient

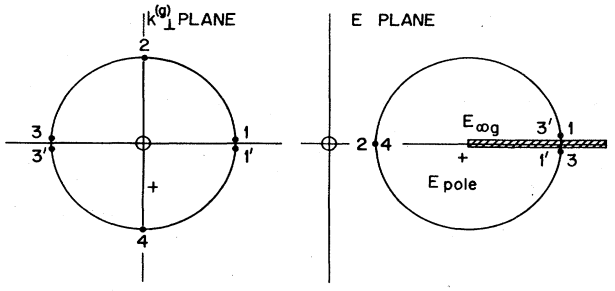

FIG. 15. Diagrams illustrating the analysis of amplitude functions. The circles are corresponding circuits on the $k_\perp^{(g)}$ plane and E plane (see text, Sec. III. A). Numbers denote representative points on these circuits. On the E plane, numbers inside the circle refer to points on the unphysical sheet. The shading denotes the branch cut and the cross denotes a pole.

$T(E)$. These singularities comprise a branch point at the beam threshold energy $E_{\infty g}$ and poles representing the resonances associated with this threshold.

The existence of the threshold branch point may be explained in physical terms as follows. The wave field of Eq. (6) is "physical" (satisfies the physically acceptable boundary condition of finiteness for $z \to -\infty$) or "unphysical" depending on the value of the square root in Eq. (8). The values of the amplitude reflection coefficient $T(E)$ are usually different in the two cases because in the physical case there is one incident wave and two reflected ones, while in the unphysical case there are two incident waves and one reflected one. At the branch point there is no difference between the two cases because $k_\perp^{(g)}$ vanishes and the third wave travels parallel to the surface. In the vicinity of the branch point, the amplitude reflection coefficient is still analytic with respect to variation of $k_\perp^{(0)}$ and so has the expansion

$$T(E) = T(E_{\infty g}) + \epsilon(E - E_{\infty g})^{1/2}, \tag{12}$$

where ϵ is a constant.

In the vicinity of the pole E_{pole}, the amplitude reflection coefficient has the form

$$T(E) = \overline{T}(E) + P/(E - E_{\text{pole}}), \tag{13}$$

where $\overline{T}$ denotes a slowly varying "background" function and P denotes the residue of the pole. At the pole, a reflected wave exists in the absence of an incident one. Thus a stationary surface state is represented by a real pole of $T(E)$. A resonance is represented by a complex pole. The possible locations of poles on the complex-energy plane are limited by the outgoing-wave condition, Eq. (9), and by the causality condition. These limitations together mean that the poles must lie on the lower half of the unphysical sheet. In other words any pole is reached from the upper half of the physical sheet by going down continuously across the real axis (Fig. 15).

For real energies E in the vicinity of an isolated pole E_{pole}, the reflection intensity $|T(E)|^2$ has a resonance fluctuation centered at $\mathrm{Re}\,E_{\text{pole}}$ and having natural width Γ given by

$$\Gamma = -2\,\mathrm{Im}\,E_{\text{pole}}. \tag{14}$$

The line shape has a characteristic form that is in general asymmetric. It may happen, however, that a resonance pole is not in fact isolated; typically there may be a sequence of resonances converging on and overlapping the corresponding beam threshold. To deal with this case in a simple way for the lowest-energy resonance, assume that the higher-energy ones can be lumped together and treated as part of the branch cut. The combined effect of the pole and branch-point singularities is then given in view of Eqs. (12 and 13) by

$$T(E) = \overline{T}(E_{\infty g}) + 1/(\alpha + \beta e^{1/2} + \gamma e), \tag{15}$$

where $e \equiv E - E_{\infty g}$ and the constants are related by

$$\alpha = P^{-1}(E_{\infty g} - E_{\text{pole}}),\quad \beta = \alpha^2\epsilon,$$
$$\gamma = [\alpha + \beta(E_{\text{pole}} - E_{\infty g})^{1/2}]/(E_{\infty g} - E_{\text{pole}}).$$

If the resonance is far from the threshold, Eq. (15) reduces to Eq. (13) and the simple pole-type line shape is obtained. However, if the resonance overlaps the threshold as it does in the case $-\mathrm{Im}E_{\text{pole}} > E_{\infty g} - \mathrm{Re}E_{\text{pole}}$, Eq. (15) indicates a substantial departure from the simple pole-type line shape due to the distorting effect of the branch point.

2. Relation between reflection and emission intensities

There is an exact relation between the electron reflection coefficients of a solid and its coefficient of thermionic emission (Herring and Nichols, 1949). A similar relation applied to any electron emission probability provided the initial distribution of electrons in the solid resembles a thermal distribution.

The exact relation may be derived as follows. Let $C(\mathbf{K})$ denote the thermionic emission coefficient and let $R(\mathbf{K}, \mathbf{K}')$ denote the intensity reflection coefficient of a crystal surface at a particular temperature. $C(\mathbf{K})d\mathbf{K}$ is the current density due to electrons emitted with momenta between $\mathbf{K}$ and $\mathbf{K}+d\mathbf{K}$. $R(\mathbf{K}, \mathbf{K}')\,d\mathbf{K}\,d\mathbf{K}'$ is the number of electrons reflected with momenta between $\mathbf{K}$ and $\mathbf{k}+d\mathbf{K}$, per incident electron with momentum between $\mathbf{K}'$ and $\mathbf{K}'+d\mathbf{K}'$. Suppose that the crystal surface forms one wall of an evacuated cavity in the bulk crystal and that thermionically emitted electrons are in thermodynamic equilibrium with the walls of the cavity. Inside the cavity the value of the current density due to electrons traveling away from the surface with momenta between $\mathbf{K}$ and $\mathbf{K}+d\mathbf{K}$ is the sum of contribution from electron emission and electron reflection. It has the expression

$$C_0(K) = C(\mathbf{K}) + \int R(\mathbf{K}, \mathbf{K}')C_0(K')\,d\mathbf{K}'. \tag{16}$$

Because of the stipulation of thermodynamic equilibrium, the total current density $C_0(K)$ due to electrons with momenta between $\mathbf{K}$ and $\mathbf{K}+d\mathbf{K}$ is independent of the direction of $\mathbf{K}$. The integral in Eq. (16) may be broken up into an integral over inelastically scattered electrons and a summation over the discrete beams in elastic scattering. Using the time-reversal relation $R(\mathbf{K}, \mathbf{K}') = R(-\mathbf{K}', -\mathbf{K})$ for elastic scattering, one obtains

$$C(\mathbf{K}) = C_0(K)\left[1 - \sum_g R_g(-\mathbf{K})\right] - \int R^{(i)}(\mathbf{K},\mathbf{K}')C_0(K')\,d\mathbf{K}', \tag{17}$$

where $R^{(i)}$ denotes an inelastic reflection coefficient and $R_g(-\mathbf{K})$ denotes the elastic reflection coefficient for incident momentum $-\mathbf{K}$ and surface-parallel momentum transfer $2\pi\mathbf{g}$. The probability of thermionic emission of an electron with momentum $\mathbf{K}$ varies linearly with one minus the total elastic reflection coefficient for incident momentum $-\mathbf{K}$.

An expression similar to Eq. (17) has been proposed to describe the relation between LEED and secondary emission intensity distributions (Feder and Pendry, 1979). The "coherent" case of secondary emission was assumed. The inelastic reflection coefficient has an approximate expression

$$R^{(i)}(\mathbf{K},\mathbf{K}') = S(\mathbf{K})Y(K') \quad K' > K \tag{18a}$$

$$= 0 \quad K' \leq K, \tag{18b}$$

where $S(\mathbf{K})$ denotes the normalized current density due to secondary electrons emitted with momenta between $\mathbf{K}$ and $\mathbf{K}+d\mathbf{K}$ and $Y(K')$ denotes the secondary yield:

$$\int_0^{K'} S(\mathbf{K})\,d\mathbf{K} = 1, \tag{19}$$

$$Y(K') = \int R^{(i)}(\mathbf{K},K')\,d\mathbf{K}. \tag{20}$$

On replacing $C(\mathbf{K})$ by $S(\mathbf{K})$ and $C_0(K)$ by $S_0(K)$ in Eq. (17) and using Eq. (18) one obtains

$$S(\mathbf{K}) = S_0'(K)\left[1 - \sum_g R_g(-\mathbf{K})\right], \tag{21}$$

$$S_0'(K) = S_0(K)/\left(1 + 4\pi\int_K^\infty S_0(K')Y(K')\,dK'\right). \tag{22}$$

The factor $S_0'(K)$ is presumably slowly varying with respect to the momentum K. Provided that the initial electron distribution induced in the crystal by the incident electrons resembles a thermal distribution, the probability of secondary emission of an electron with momentum $\mathbf{K}$ is nearly proportional to one minus the elastic reflection coefficient for incident electrons with momentum $-\mathbf{K}$.

B. Description using 2-D Fourier expansions

The description has as a starting point the 2-D Fourier expansion of both the electron wave field and the scattering potential of the crystal. By this means the Schrödinger equation for an electron moving in a 2-D periodic potential is reduced to a set of coupled ordinary differential equations. From a formal viewpoint, the theory may be identified as a special case of a general treatment of scattering given by Feshbach (1958) in a paper entitled "Unified Theory of Nuclear Reactions." In this application to the surface resonance band structure, the theory is the 2-D analog of the nearly-free-electron theory of bulk crystal band structure.

1. Simplified treatment of elastic scattering

In Feshbach's treatment of scattering, the wave function for the entire system, incident particle and target, is expanded

$$\Psi = \sum_j u_j f_j, \tag{23}$$

where f_j is a wave function describing the jth state of the target and u_j is a function of the coordinates of the incident particle. Each of the indices j labels a scattering "channel." In the case of elastic electron-surface scattering, the expression corresponding to the summation in Eq. (23) is the 2-D Fourier expansion of the electron wave field for a given value of $(E,\mathbf{k}_{\|})$:

$$\sum_g u_g(z)\exp\left[i(\mathbf{k}_{\|} + 2\pi\mathbf{g})\cdot\mathbf{r}\right]. \tag{24}$$

Formally, the role of the jth "target" state f_j in Feshbach's theory is taken by a function representing free-electron motion parallel to the surface with momentum $\mathbf{k}_{\|} + 2\pi\mathbf{g}$. The "target" coordinates are replaced by the electron position vector projection $\mathbf{r}$ parallel to the surface. The "particle" coordinates are replaced by the inward surface normal electron coordinate z. The channel index is the reciprocal-net vector $\mathbf{g}$. For each value of $\mathbf{g}$ there is one pair of diffraction beams—one ingoing beam and one outgoing beam. Thus in the case of elastic scattering there is a one-to-one correspondence between channels and pairs of diffraction beams. "Open" and "closed" channels correspond respectively to propagating and nonpropagating or evanescent beams. The target energy eigenvalues correspond to beam threshold energies. By taking account of these correspondences, all theoretical results for elastic electron surface scattering may be obtained by a straightforward transcription of Feshbach's formulas.

The essential elements of the theory using 2-D Fourier expansions may be introduced for a simplified case where (i) The expression for the wave field, Eq. (24), contains two terms only, and (ii) The resonance is isolated—i.e., there are no branch points or other resonance poles in the vicinity of the pole considered explicitly.

Suppose that one of the terms in Eq. (24) corresponds to an open channel labeled by reciprocal-net vector 0 while the other term corresponds to a closed channel labeled by $\mathbf{g}$. By substituting Eq. (24) into the Schrödinger equation and integrating over the coordinates $\mathbf{r}$, one obtains the coupled equations

$$(V_\perp + U_0 + E_{\infty 0} - E)u_0 = -U_{-g}u_g, \tag{25a}$$

$$(V_\perp + U_0 + E_{\infty g} - E)u_g = -U_g u_0, \tag{25b}$$

where $V_\perp$ is the kinetic energy operator for the surface-normal coordinate, $E_{\infty 0}$ and $E_{\infty g}$ are threshold energies, and $U_g(z)$ denotes a Fourier coefficient of the potential $U(z,\mathbf{r})$:

$$U_g(z) = A^{-1}\int \exp(-i2\pi\mathbf{g}\cdot\mathbf{r})U(z,\mathbf{r})\,d\mathbf{r}. \tag{26}$$

The integration is over one unit mesh of area A.

The required solutions of the equation system Eq. (25) are those having the following asymptoic forms far out-

side the crystal ($\lim z \to -\infty$):

$$u_0(z) \sim (k_\perp^{(0)})^{-1/2}[\exp(ik_\perp^{(0)}z) + T_0 \exp(-ik_\perp^{(0)}z)], \quad (27)$$

$$u_g(z) \sim \exp(-ik_\perp^{(g)}z). \quad (28)$$

The normal momentum components are as defined in Eqs. (7) and (8) and satisfy the conditions of Eqs. (9) and (10).

The electron wave field outside the crystal will usually be described quite well by solutions of the homogeneous equation corresponding to Eq. (25a). However, if $u_g(z)$ resembles a bound-state solution of the homogeneous equation corresponding to Eq. (25b)—i.e., if $u_g(z)$ resembles a surface state for the potential $U_0(z)$—then the magnitude of the inhomogeneity $-U_{-g}u_g$ in Eq. (25a) may assume relatively large values. In this way the wave field outside the crystal is perturbed under approximately the conditions for existence of surface states.

A formulation of the above idea may be obtained following Feshbach by first of all introducing a formal expression for the closed-channel function into Eq. (25a) to give

$$(H_{00} - E)u_0 = -U_{-g}[1/(E + i\eta - H_{gg})]\, U_g u_0. \quad (29)$$

Here H_{00} stands for $V_\perp + U_0 + E_{\infty 0}$, H_{gg} has an analogous meaning, and $\eta \to +0$ is specified to satisfy the outgoing-wave condition, Eq. (9). The next step is to introduce the spectral representation of the operator in Eq. (29) using the eigenfunctions of the operator $V_\perp + U_0$. The eigenfunction spectrum consists in general of a set of discrete bound-state functions $\psi_{n'}(z)$ with energy eigenvalues $e_{n'}$ and a contiuum $\psi(\epsilon, z)$ with energies ϵ. The spectral representation is

$$\frac{1}{E + i\eta - H_{gg}} = \sum_{n'} \frac{|\psi_{n'}\rangle\langle\psi_{n'}|}{E - E_{\infty g} - e_{n'}} + \int_0^\infty \frac{|\psi(\epsilon)\rangle\langle\psi(\epsilon)|\, d\epsilon}{E + i\eta - E_{\infty g} - \epsilon}. \quad (30)$$

The assumption of an isolated resonance may now be introduced to simplify subsequent calculation. For energies E close to one of the bound-state energies $E_{ng} = E_{\infty g} + e_n$, it is a good approximation to keep only the term $n' = n$ from Eq. (30) on the right side of Eq. (29), replacing E by E_{ng} in the remainder and lumping it with U_0 to give an effective potential $U_0^{(n)}$ and Hamiltonian $H_{00}^{(n)}$ on the left side. This yields

$$(H_{00}^{(n)} - E)\, u_0 = -\Lambda_n U_{-g}\psi_n \quad (31)$$

with

$$\Lambda_n \equiv \langle \psi_n U_g u_0\rangle/(E - E_{ng}). \quad (32)$$

To complete the calculation of Λ_n, the formal expression for u_0, namely

$$u_0 = \nu_0 + \Lambda_n (E + i\eta - H_{00}^{(n)})^{-1} U_{-g}\psi_n, \quad (33)$$

is introduced into Eq. (32) to yield:

$$\Lambda_n = \langle \psi_n U_g \nu_0\rangle/(E - E_{ng} - \Delta E_{ng}), \quad (34)$$

$$\Delta E_{ng} = \langle \psi_n U_g (E + i\eta - H_{00}^{(n)})^{-1} U_{-g}\psi_n\rangle. \quad (35)$$

In Eqs. (33 and 34), ν_0 denotes the solution for the homogeneous equation corresponding to Eq. (31) that is asymptotically ($z \to -\infty$):

$$\nu_0(z) \sim (k_\perp^{(0)})^{-1/2}[\exp(ik_\perp^{(0)}z) + T_0^{(n)} \exp(-ik_\perp^{(0)}z)]. \quad (36)$$

It represents the incident wave plus an outgoing wave due to the potential $U_0^{(n)}$.

The final step is to obtain an expression for the amplitude reflection coefficient T_0 from the asymptotic expression for the wave field. The required expression is obtained from Eq. (33) using

$$(E + i\eta - H_{00}^{(n)})^{-1} \sim |\exp(-ik_\perp^{(0)}z)\rangle\langle\nu_0(z)|, \quad (37)$$

and the result is

$$T_0 = T_0^{(n)} + \langle \nu_0 U_{-g}\psi_n\rangle\langle\psi_n U_g \nu_0\rangle/(E - E_{ng} - \Delta E_{ng}). \quad (38)$$

The second term on the right of Eq. (38) represents the resonance contribution to the reflection amplitude. The numerator is the product of the probability amplitudes for the transition from a propagating ingoing state to a surface state and the transition from the surface state to a propagating outgoing state. These transitions result from interactions designated as type 1 in Fig. 3. The resonance amplitude contribution is centered at energy $E_{ng} + \mathrm{Re}\Delta E_{ng}$. It has natural width $\Gamma = -2\,\mathrm{Im}\Delta E_{ng}$ [cf. Eq. (14)]. ΔE_{ng} is the perturbation of the surface-state energy E_{ng} due to interactions with the continuum of propagating states (to see this use the spectral representation of the operator in the expression for ΔE_{ng}). This interaction is of type 2 in Fig. 3.

2. Extensions of simplified treatment

The simplified treatment takes account of only one closed channel. It may be extended to include many closed channels by replacing the operator H_{00} by the matrix operator

$$H_{gg'} = V_1 \delta_{gg'} + U_{g-g'} + E_{\infty g}\delta_{gg'}. \quad (39)$$

Interactions between different zeroth-order bound states ψ_n (interactions of type 3, Fig. 3) may occur because of the off-diagonal elements of this operator. The resonance denominator must be changed to $E - E_p - \Delta E_p$ where E_p is an eigenvalue of $H_{gg'}$, and ΔE_p is an energy displacement analogous to ΔE_{ng} in Eq. (38).

Another kind of extension is required to deal with the indirect effect of inelastic channels on the elastic scattering amplitude. These inelastic channels may be taken into account as "absorption" of the elastic wave field by assigning a positive imaginary part to the potential $U^{(n)}$. The resulting complex potential is usually called "optical potential." The elastic decay of the surface state to propagating Bloch waves is indistinguishable from inelastic scattering and may be treated as absorption in calculations of reflection intensities.

Finally the simplified theory may be extended to deal with the case where there is more than one open channel. For example, if there is an open elastic channel g′ in addition to the open channel 0 and closed channel g, the reflection amplitudes for scattering into these channels have the expressions

$$T_0 = T_0^{(n)} + \langle \nu_0 U_{-g}\psi_n\rangle\langle\psi_n U_g \nu_0\rangle/(E - E_{ng} - \Delta E_{ng}), \quad (40)$$

and

$$T_{g'} = T_{g'}^{(n)} + \langle \nu_{g'} U_{g'-g}\psi_n\rangle\langle\psi_n U_g \nu_0\rangle/(E - E_{ng} - \Delta E_{ng}), \quad (41)$$

where ΔE_{ng} has a meaning similar to that indicated by

Eq. (35):

$$\Delta E_{ng} = \langle \psi_n U_g (E + i\eta - H_{00}^{(n)})^{-1} U_{-g} \psi_n \rangle + \langle \psi_n U_{g-g'} (E + i\eta - H_{00}^{(n)})^{-1} U_{g'-g} \psi_n \rangle , \quad (42)$$

and $\nu_{g'}$ is the solution of

$$(V_\perp + U_0 + E_{\infty g'} - E) u_{g'} = 0 \quad (43)$$

that is asymptotically ($z \to -\infty$)

$$\nu_{g'}(z) \sim (k_\perp^{(g')})^{-1/2} T_{g'}^{(\eta)} \exp(-ik_\perp^{(g')} z) . \quad (44)$$

The important points are that the resonance denominators are the same for the two channels, but the resonance numerators differ with respect to the probability amplitude for transitions from the surface state to the final outgoing state.

The above remarks apply to elastic scattering, but a similar description applies to inelastic scattering as well. To treat inelastic scattering in channel g′ with energy loss δE, all equations and definitions of the previous paragraph apply except for replacement of $E_{ng'}$ by $E_{ng'} - \delta E$ in Eq. (43) and in the definition of the normal component $k_\perp^{(g')}$ of the propagation vector.

3. 2-D nearly-free-electron scheme

The surface resonance band structure may be calculated approximately by a perturbation scheme based on the 2-D free-electron functions

$$|ng\rangle = \psi_n(z) \exp[i(\mathbf{k}_\parallel + 2\pi \mathbf{g}) \cdot \mathbf{r}] . \quad (45)$$

This is called the 2-D nearly-free-electron scheme. Starting with the Hamiltonian $H = T_\perp + T_\parallel + U(z, \mathbf{r})$, where $T_\parallel$ is the surface-parallel kinetic energy operator, one has the energy matrix

$$\langle ng|H|n'g'\rangle = \int_{-\infty}^{\infty} \psi_n^*(z) H_{gg'}(z) \psi_n(z) dz , \quad (46)$$

where $H_{gg'}$ results from integration over surface-parallel coordinates and has the expression given in Eq. (39). The eigenvalues of the energy matrix Eq. (46) are identical with the approximate resonance energies E_p in the Feshbach theory for many closed channels—i.e., they are resonance energies calculated neglecting interactions with the continuum.

A useful approximation to the energy matrix may be found from the following gross properties of the functions $\psi_n(z)$. These functions are bound-state eigenfunctions of the Hamiltonian $T_\perp + U_0$. Their gross properties depend on the shape of the potential in the surface region near and outside the outermost atom layer of the substrate crystal. A convenient description of this situation is obtained by dividing the potential into "surface" and "bulk" parts at a suitably positioned plane $z = 0$. In the case of a metal crystal surface, the boundary plane can be chosen so that in an approximation good enough for the present purpose the "surface" potential has the image form $1/4z$ ($z < 0$) while the "bulk" potential is a periodic function of z. The required wave functions are solutions of the Schrödinger equation for the image potential that vanish for $z \to -\infty$ and join smoothly to the bulk wave functions at $z = 0$. The nature of the boundary condition at $z = 0$ is not important for the present discussion. It suffices to treat only one

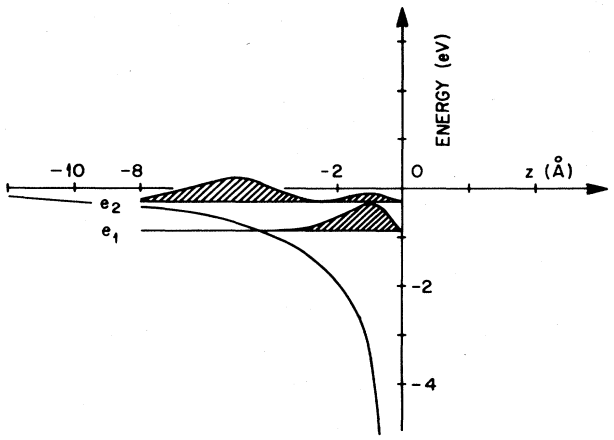

FIG. 16. Plot of the image potential with energy levels and electron density distributions (shaded plots) corresponding to the boundary condition that the wave function vanish at the origin.

case, namely that for which the bulk wave function vanishes at $z = 0$. In that case the Schrödinger equation is the same as the $l = 0$ radial equation for the hydrogen atom, where the radial coordinate is replaced by $2z$. The binding energies are given by $-e_n = 1/32n^2$. The energy levels and electron density distributions $|\psi_n(z)|^2$ for $n = 1$ and 2 are sketched in Fig. 16.

Two points bearing on the energy matrix stand out clearly from Fig. 16. First, the overlap between wave functions with different indices n is small. Second, wave functions with indices $n > 1$ have relatively weak overlap with the bulk potential. It follows (at least for metals) that by far the most important off-diagonal matrix elements $\langle ng|H|n'g'\rangle$ are those for which $n' = n = 1$. The energy matrix reduces approximately to

$$\langle 1g|H|1g'\rangle = \langle U_{g-g'} \rangle \equiv \int_{-\infty}^{\infty} \psi_1^* U_{g-g'} \psi_1 dz , \quad (g' \neq g) \quad (47a)$$

$$= e_1 + E_{\infty g} , \quad (g' = g) . \quad (47b)$$

The quantity $\langle U_{g-g'} \rangle$ is the $(g - g')$th Fourier component of the "surface-weighted potential"—i.e., the potential weighted with respect to the electron density of the $n = 1$ resonance.

The 2-D nearly-free-electron description reduces to the 2-D free-electron one if the off-diagonal elements are comparatively small, i.e., if the following inequality is satisfied:

$$|\langle U_{g-g'} \rangle| \ll |E_{\infty g} - E_{\infty g'}| , \quad (g \neq g') . \quad (48)$$

On the other hand the lateral variation of the surface-weighted potential causes comparatively large displacements of degenerate or nearly degenerate 2-D free-electron levels such as occur for $\mathbf{k}_\parallel$ values near the crossings of different branches of the free-electron band structure.

The interactions between 2-D free-electron levels are generally accompanied by systematic variations of resonance intensities. These trends can be related to selection rules based on elementary symmetry properties. As is apparent from the form of the resonance numera-

tor in Eq. (38), the only "allowed" resonances are those having the same symmetry as the incident wave field under the point-group operations of the surfaces. For example, suppose that the reciprocal-net vectors g and g′ are related as mirror images with respect to the plane containing the incident beam and the surface normal. The interaction between the 2-D free-electron states $|1g\rangle$ and $|1g'\rangle$ results in resonances with wave functions and energies

$$|1g\rangle \pm |1g'\rangle, \quad e_1 \pm \langle U_{g-g'} \rangle . \tag{49}$$

In this case the symmetric (+) combination is "allowed" and the antisymmetric (–) one is "forbidden" by symmetry.

C. Layer multiple-scattering description

The elastic scattering of electrons at a crystal surface may be described as multiple scattering between two "layers" of potential that correspond respectively to the surface region and the bulk crystal (Artmann, 1947; McRae, 1971). In principle the mode of division of the crystal into these two regions is arbitrary but the practical advantages of the description depend on choosing a suitable dividing surface. A popular choice is to terminate the bulk crystal by a plane located one-half of one atom-layer spacing outside the center of its outermost atom layer. This choice is illustrated in Fig. 2. The origin plane $z = 0$ is chosen to coincide with the termination of the bulk crystal, so that the surface region lies to the left of the origin. The division of the crystal into bulk and surface regions inevitably calls for a degree of idealization of the potential. This is indicated by broken lines in Fig. 2.

1. Simplified treatment

The essential elements of the layer multiple-scattering description may be introduced for a simplified case where only two pairs of diffraction beams are considered (four-beam case). In this case, an expression for the scattering amplitude is obtained by summing over chains of diffraction processes such as those indicated in Fig. 17. In Fig. 17, S and T^0 are scattering amplitude factors for the surface and bulk regions, respectively. Subscripts gg' refer to the diffraction process with parallel-momentum change $2\pi(g' - g)$. Superscripts I, II, . . . , denote transmission or reflection amplitudes at the surface region as indicated in the figure. All of the amplitude coefficients are functions of E and $k_{\parallel}$.

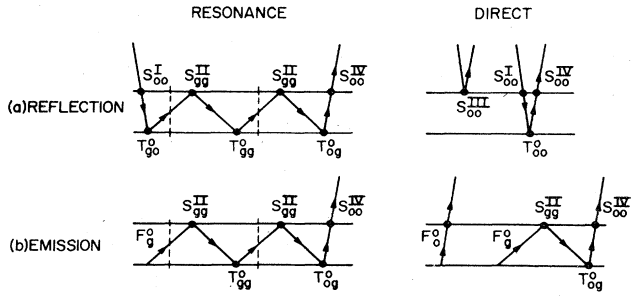

FIG. 17. Decomposition of resonance scattering into diffraction processes. In each of the four diagrams, upper and lower horizontal lines represent the surface and bulk regions, respectively. Filled circles denote diffraction events. The sequences of events indicated between broken lines can be repeated to generate chains of diffraction processes. The notations are those used in the text, Sec. III.C.

Consider the case of electron reflection represented by Fig. 17(a). Fig. 17(a) corresponds to the elastic reflection case of Fig. 4(a). The resonance contribution to the specular reflection amplitude T_{00} is obtained by summing terms such as

$$S_{00}^{\mathrm{IV}} T_{0g}^{o} S_{gg}^{\mathrm{II}} (T_{gg}^{o} S_{gg}^{\mathrm{II}})^{j} T_{g0}^{o} S_{00}^{\mathrm{I}} \quad j = 0, 1, \ldots .$$

Summing over resonance terms and adding in the corresponding direct contribution gives

$$T_{00} = S_{00}^{\mathrm{III}} + S_{00}^{\mathrm{IV}} T_{00}^{0} S_{00}^{\mathrm{I}} + S_{00}^{\mathrm{IV}} T_{0g}^{0} S_{gg}^{\mathrm{II}} T_{g0}^{0} S_{00}^{\mathrm{I}} / (1 - T_{gg}^{0} S_{gg}^{\mathrm{II}}) . \tag{50}$$

The direct term and a factor of the resonance numerator are relatively slowly varying functions of $(E, \mathbf{k}_{\parallel})$, so the amplitude reflection coefficient has the form

$$T = C[1 + RS/(1 - T^0 S)] , \tag{51}$$

where C and R are slowly varying and unnecessary subscripts and superscripts are omitted.

A similar treatment applies to electron emission. The emission amplitude may be calculated by summing over chains of diffraction processes such as those indicated in Fig. 17(b). Figure 17(b) corresponds to the elastic resonance case of Fig. 4(c). Let F_g denote the amplitude of emission from the crystal for electrons with parallel momentum $\mathbf{k}_{\parallel} + 2\pi\mathbf{g}$, and let F_g^0 denote the corresponding quantity for the bulk. A derivation similar to that of Eq. (51) gives

$$F = C[RS/(1 - T^0 S)] \tag{52}$$

where however the slowly varying terms represented by C and R are now

$$S^{\mathrm{IV}} F_0^0 \text{ and } S_{00}^{\mathrm{IV}} T_{0g}^{0} F_g^0 / C ,$$

respectively.

As is apparent from Eqs. (51 and 52) the resonance energy for given value of $k_{\parallel}$ is the energy at which the magnitude of the resonance denominator $1 - T^0 S$ is at a minimum. The energy dependence of the resonance denominator can be understood readily in a hypothetical case. Suppose that the scattering is purely elastic and that off-diagonal diffraction amplitudes such as T_{0g}^0 all vanish. Then $S \equiv S_{gg}^{\mathrm{II}}$ is of modulus unity for all energies less than the threshold energy $E_{\infty g}$, and $T^0 \equiv T_{gg}^0$ is also of modulus unity across each forbidden gap. The value of the resonance denominator then depends entirely on the phase of the product $T^0 S$. The resonance denominator vanishes at the energies E_{ng}, identical with 2-D free-electron energies, for which the following phase condition is satisfied:

$$\tau + \sigma = 2n, \quad n = 1, 2, \ldots , \tag{53}$$

where $\tau \equiv \pi^{-1} \arg T^0$ and $\sigma \equiv \pi^{-1} \arg S$. Physically, Eq. (53) means that the phase advance of an electron wave in each cycle of multiple scattering between the surface and bulk regions is an integer multiple of 2π. Thus there exist states of sustained multiple scattering or

stationary bound states with energies E_{ng}.

In the above hypothetical case, each stationary state corresponds to a resonance that has zero width (since the resonance denominator vanishes) and zero resonance numerator [the resonance numerator R in Eqs. (51) and (52) is proportional to off-diagonal diffraction amplitudes such as T^0_{0g}]. If, however, the off-diagonal diffraction amplitudes are taken into account, the product T^0S must satisfy the unitarity condition $|T^0S|<1$. The resonance energy is still given approximately by Eq. (53), but the resonance necessarily has nonzero width due to the interaction of the discrete state with the continuum. An expression for the characteristic width of the resonance may be obtained by expanding the resonance denominator $1-T^0S$ about the resonance energy E_{ng} and using Eq. (14). This gives for the width (assuming $|T^0S|$ independent of energy)

$$\Gamma_{ng}=2(1-|T^0S|)/[\,|T^0S|\,\pi(d\tau/dE+d\sigma/dE)|_{E_{ng}}\,]. \quad (54)$$

Further reduction of $|T^0S|$ with broadening of the resonance results in general from inelastic scattering. Thus in Eqs. (51 and 52), inelastic scattering may be represented phenomenologically by adjusting the value of $|T^0S|$.

2. General treatment

The simplified treatment described above can be extended to take account of all possible chains of diffraction processes of the type shown in Fig. 17 (McRae, 1971). A matrix notation is useful for this purpose. In the reflection case, for example, the matrix of amplitude coefficients $T_{gg'}$ may be calculated by steps analogous to those leading to Eq. (50). The result is

$$T=S^{III}+S^{IV}T^0S^I+S^{IV}T^0S^{II}(I-T^0S^{II})^{-1}T^0S^I, \quad (55)$$

where I is the unit matrix and other symbols stand for matrix analogs of the amplitude coefficients in Eq, (50). In terms of the eigenvalue representation of the matrix T^0S^{II}—

$$T^0S^{II}U=U\Lambda, \quad (56)$$

where Λ is a diagonal matrix—Eq. (55) may be written

$$T_{gg'}=C_{gg'}+\sum_h \frac{A_{gh}B_{hg'}}{1-\Lambda_h}. \quad (57)$$

Here C is the direct part and A and B stand for matrices

$$S^{IV}T^0S^{II}U \text{ and } U^{-1}T^0S^I,$$

respectively. Equation (57) differs from the one originally published (McRae, 1971) with regard to the division into direct and resonance contributions.

The general description is of the same form as the simplified one but calls for replacement of each term such as $T^0_{gg}S^{II}_{gg}$ in Eq. (50) by an eigenvalue Λ of the matrix T^0S^{II}.

The surface resonance band structure is to be found by mapping the $(E,\mathbf{k}_{\parallel})$ values at the minima of

$$|\det[I-T^0S^{II}]|. \quad (58)$$

Under certain conditions it is a good approximation to replace the matrix T^0S^{II} by a single term such as $T^0_{gg}S^{II}_{gg}$. In this case one recovers the simplified treatment described under heading 1. above. The conditions are

(i) The off-diagonal elements of T^0S^{II} are comparatively small so that the inequality

$$\left|\sum_{g''} T^0_{gg''}S^{II}_{g''g'}\right| \ll \left|\sum_{g''} T^0_{gg''}S^{II}_{g''g}-\sum_{g''} T^0_{g'g''}S^{II}_{g''g'}\right| \quad (g\neq g') \quad (59)$$

is satisfied for all reciprocal-net vectors g and g', and

(ii) The lateral variation of potential in the surface region is weak so that the off-diagonal elements of S^{II} are comparatively small.

If (i) is satisfied the eigenvalues are approximately equal to the diagonal elements, and if (ii) is satisfied the diagonal elements are approximately products such as $T^0_{gg}S^{II}_{gg}$. These conditions are satisfied or not in the same circumstances as is the corresponding condition for the 2-D nearly-free-electron description, Eq. (48). In particular, near a crossing of the branches $E_{\infty g}$ and $E_{\infty g'}$ of the 2-D free-electron band structure, each of the terms on the right of Eq. (59) approaches unity and so their difference is comparatively small.

3. Results for the image potential

Applications of the simplified layer multiple-scattering treatment to the image potential $1/4z$ $(z<0)$ offer a preliminary estimate of resonance energies, widths, and line shapes for metals. The simplified treatment gives expressions relating these quantities to the surface reflection phase parameter $\sigma\equiv\pi^{-1}\arg S$ and the bulk reflection phase parameter $\tau\equiv\pi^{-1}\arg T^0$. As before S and T^0 denote amplitude reflection coefficients for the resonant wave at the surface and bulk, respectively. In applications of the simplified treatment, the slowly varying quantities C, R, and $|T^0S|$ are replaced by constants. Thus the results depend only on the variation of the phase parameters with energy.

The energy dependence of the surface reflection phase parameter for the image potential has the expression

$$\sigma(e)=\tfrac{1}{2}(-2e)^{-1/2}-1 \quad (60)$$

where e denotes the energy referred to the threshold in question—e.g., $e\equiv E-E_{\infty g}$ for the gth threshold (McRae, 1979).

In the absence of detailed information about its energy dependence, the value of the reflection phase τ is assumed to be constant. The meaning of this assumption can be understood from results of the "two-beam" description of reflection electron diffraction, which is equivalent to a one-dimensional model. For a one-dimensional crystal terminated in the manner indicated in Fig. 2, the value of τ increases by 1 on crossing a forbidden gap. The value goes from 0 to 1 or from 1 to 2 depending on the ordinal number of the gap (McRae, 1971). The small amount of experimental information that is available for real crystals appears to indicate that the increase of τ on crossing a gap is indeed of order 1 (McRae, 1975). The assumption of a constant τ is thus valid for the "wide-gap" case in which the width of the gap is much larger than the binding energy of the lowest-energy resonance.

By inserting Eq. (60) into Eq. (51) the reflection amplitude is found to be ($\rho \equiv \pi^{-1} \arg R$)

$$T(e) = C\left[1 + \frac{|RS| \exp\{i\pi[\rho + \frac{1}{2}(-2e)^{-1/2} - 1]\}}{1 - |T^0 S| \exp\{i\pi[\tau + \frac{1}{2}(-2e)^{-1/2} - 1]\}}\right]. \tag{61}$$

By inserting Eq. (60) into Eq. (53) the binding energy for the nth resonance is found to be

$$-e_n = 1/[32(n+a)^2], \tag{62}$$

where the "quantum defect" a is $-\frac{1}{2}(\tau - 1)$. Equation (62) (with an unspecified constant a) was derived by Rundgren and Malmström (1977a). It shows that the resonance energies form a modified hydrogenic series converging on the beam threshold. If the wave function vanishes at the origin, the bulk reflection phase τ is 1 and the hydrogenic series shown in Fig. 16 is recovered. As the possible values of τ range for 0 to 2, the values of the binding energy of the $n=1$ level allowed by the model range from $\frac{1}{72}$ to $\frac{1}{8}$ hartree (from 0.4 to 3.4 eV).

By inserting Eq. (60) into Eq. (54) and taking $|T^0 S|$ to be a constant, the characteristic width Γ_n of the nth resonance is found to be

$$\Gamma_n = 2(1 - |T^0 S|)/[|T^0 S| 32\pi (n+a)^3]. \tag{63}$$

The $n=1$ resonance can be resolved as long as its width is less than about twice its binding energy. By comparing Eqs. (62) and (63) the criterion for resolution of the $n=1$ resonance is found to be approximately $|T^0 S| > [1 + \pi(1+a)]^{-1}$. As n increases, the resonance widths decrease at the same rate as the mean level separation from neighboring resonances. Therefore, for a constant value of $|T^0 S|$ satisfying the above criterion, all resonances converging on a given threshold are in principle resolvable. This result was derived by Pendry and Echenique (1978).

One does not expect the value of $|T^0 S|$ to be quite constant as assumed for the above derivation. The magnitude of the surface reflection coefficient S is reduced by inelastic scattering or "absorption" in the surface region. There is theoretical evidence (Inkson, 1973) and experimental evidence (McRae and Caldwell, 1976b) that the range of the absorptive potential representing inelastic scattering at metal surfaces is much smaller than the range of the image potential. On going to higher-order resonances, the resonance electron density has progressively weaker overlap with the absorptive potential. Consequently, as the order number increases, $|S|$ should increase with a corresponding reduction of resonance widths. The extent to which the value of $|S|$ for the $n=1$ resonance is reduced by inelastic scattering depends on the overlap of the electron density distribution $|\psi_1(z)|^2$ with the absorptive potential. This in turn depends on the value of the bulk reflection phase τ. In the vicinity of the plane $z=0$ bounding the bulk crystal, the resonance wave function has the form

$$\psi_1(z) \approx |T^0| \exp[i(\tau\pi - k_\perp z)] + \exp(ik_\perp z) \tag{64}$$

required to match the bulk crystal wave function (T^0 denotes the amplitude coefficient of reflection and $k_\perp$ denotes the inward surface-normal component of electron momentum). Ordinarily the maximum of the density distribution $|\psi_1(z)|^2$ lies outside the $z=0$ plane as shown in an extreme case ($\tau = 1$) in Fig. 16. But as shown by Eq. (64), as τ approaches 0 or 2 the maximum moves towards the bulk crystal and up to the $z=0$ plane. Thus the broadening effect of inelastic scattering is at a maximum for $\tau = 0$ or 2.

The above results for the image potential are derived by the simplified layer multiple-scattering treatment and so omit perturbations due to off-diagonal elements of the matrix $T^0 S^{II}$. In a first approximation, however, the effects of these perturbations can be accommodated merely by changing the value of the constant τ. Thus Eqs. (61)-(63) can be used to fit experimental data even if there is evidence of interaction between 2-D free-electron states, but in that case τ will not have exactly the meaning of the bulk reflection phase parameter.

While the image potential is a useful starting point for the interpretation of resonances, at least three modifications are needed for quantitative calculations. First, the correct form of potential at large distances from the surface is $1/4(z - z_0)$ where according to calculations (Appelbaum and Hamann, 1972; Lang and Kohn, 1973) the image potential origin z_0 is located about 1 a.u. (1 a.u. = 0.53 Å) to the vacuum side of the bulk crystal termination indicated in Fig. 2. Second, exchange and correlation effects are known to be quite important at distances within about 2 a.u. of the bulk termination (Lang and Kohn, 1970, 1971) and so could affect resonance energy levels, including especially the $n=1$ level. These theoretically expected modifications of the image potential were taken into account in calculations of resonance intensity curves by Read and Jennings (1978) (see Sec. III.D). The third point is that because of retardation of the polarization of the crystal in response to the incident electron, the actual potential should become progressively weaker than the image potential on going to higher energies. The chief retardation effect will arise from the electron velocity component parallel to the surface. This case has been discussed theoretically (Harris and Jones, 1974) but quanitative estimates are lacking.

4. Comparison with 2-D Fourier transform description

The layer multiple scattering and 2-D Fourier transform descriptions have complementary advantages and disadvantages.

The 2-D Fourier transform description is well adapted to the semiempirical representation of the surface resonance band structure. It can be applied to inelastic as well as elastic scattering amplitudes. Its disadvantage is that it yields a simple form for the reflection amplitude only for the "isolated resonance" case; thus it does not offer any convenient way of visualizing the effects of overlapping resonances and branch points.

The layer multiple-scattering description has a practical advantage for model computations since some of the quantities involved such as the bulk reflection amplitude are already programmed for LEED intensities. A disadvantage is that the use of a scattering matrix rather than an energy matrix makes it difficult to visualize the surface resonance band structure. On the other hand, the amplitude expression retains the correct

analytic form in all approximations [cf. Eq. (15)] so that the effects of overlapping resonances and branch points are readily included.

D. Applications and comparison with experiment

1. Intensity curves

Calculations of intensity curves containing resonance features were reported by Read and Jennings (1978) and by Jennings and co-workers in earlier publications (Jennings and Read, 1974, and references given by them). The layer multiple-scattering method was applied to the calculation of LEED intensities at clean metal (001) surfaces. The bulk reflection matrix was calculated as in standard LEED intensity analysis (Pendry, 1974) but a more detailed treatment was applied to the surface scattering. The standard LEED procedure uses "no-reflection" boundary conditions equivalent to neglecting the off-diagonal elements of the surface scattering matrix. This provision artifically suppresses all resonance structure. In the calculations of Jennings and co-workers the scattering matrix was calculated exactly for assumed one-dimensional potentials in the surface region. This made it possible to study the effect of varying potential parameters on resonance positions and lineshapes. Results obtained with the image potential and various modifications of it were reported. Using a modified image potential joining smoothly to the bulk crystal potential, Read and Jennings varied the image-potential origin z_0 to bring the calculated resonance profile for Cu(001) surface into agreement with LEED observations (Andersson, 1970). The results confirmed that the image-potential origin is about 1 a.u. outside the bulk crystal termination. Calculations of a similar type, again for metal (001) surfaces but on a finer scale to show detailed resonance structure, were reported by Rundgren and Malmström (1977a,b) and by Jennings (1978). So far all theoretical calculations of intensity curves have been limited to what in this article is called the 2-D free-electron description—in other words the interactions between resonances deriving from different thresholds have not been taken into account in a full-scale calculation.

2. Surface resonance band structure

In addition to calculations of intensity curves, there have been several calculations dealing specifically with the surface resonance band structure by methods already established for surface states near the Fermi level. In this category may be cited publications by Smith and Mattheiss (1976) (for comparison with experiment see Sec. IV.B of the present article), by Bisi, Calandra, and Manghi (1977) and by Schlüter and Cohen (1978) (see Sec. II.B). All of these calculations neglect the long-range potential and thus refer to the "strong overlap" type of resonance (Sec. II.A).

Another approach to the interpretation of surface resonance band structure is the semiempirical one introduced by McRae, Landwehr, and Caldwell (1977). The treatment is based on the 2-D nearly-free-electron scheme (Sec. III.B). If used in a purely theoretical calculation of the surface band structure, this scheme would require the use of a pseudopotential to obtain convergence. In a semiempirical application, however, the procedure is inverted to extract a pseudopotential from a fit to experimental data. The fit is obtained by adjusting the values of the binding energy and of a small number of off-diagonal elements of the energy matrix. The interaction elements so evaluated may be identified with Fourier coefficients $\langle U_g \rangle$ of a surface-weighted pseudopotential defined by

$$\langle U(\mathbf{r}) \rangle \equiv \int_{-\infty}^{\infty} \psi_1^*(z)\, U(z, \mathbf{r}) \psi_1(z)\, dz\,,$$

where $U(z, \mathbf{r})$ denotes the pseudopotential and the notation is otherwise as in Sec. III.B. Thus the surface-weighted pseudopotential may be synthesized from its empirically determined components according to

$$\langle U(\mathbf{r}) \rangle = \sum_{g} \langle U_g \rangle \exp(i 2\pi \mathbf{g} \cdot \mathbf{r})\,. \tag{65}$$

3. Temperature dependence of elastic reflection intensities

Calculations were reported for the MgO(001) surface (Kawamura, Ohkawa, and Miyake, 1976) and gave good account of resonance intensity measurements for that surface (Wada, Suzuki, and Ichnokawa, 1976).

The idea underlying the calculations is that for a diffraction beam corresponding to electron momentum transfer H, the intensity $I(\mathrm{H})$ as given in the kinematic (single-scattering) approximation is proportional to $\exp[-2M(\mathrm{H})]$, where $M(\mathrm{H})$ is a temperature dependent Debye–Waller parameter whose momentum dependence is

$$M(\mathrm{H}) \propto |\mathbf{H}|^2\,. \tag{66}$$

However, for a reflection resonance scattering process involving two successive momentum transfers G and H − G as illustrated in Fig. 18, the effective Debye–Waller parameter is given by

$$M'(\mathrm{H}) = M(\mathrm{G}) + M(\mathrm{H} - \mathrm{G}) \propto |\mathbf{G}|^2 + |\mathbf{H} - \mathbf{G}|^2\,, \tag{67}$$

which is in general different from $M(\mathrm{H})$. For example, if H is normal to the surface and the normal component of G is larger than the parallel one as shown in Fig. 18, then the effective Debye–Waller factors satisfy $M'(\mathrm{H}) < M(\mathrm{H})$ and the temperature dependence of intensity at the resonance is relatively weak.

Another and completely different perturbation of temperature dependence can arise from the variation of the depth of the crystal sampled by incident electrons with respect to incidence conditions near a resonance. For incidence conditions close to a resonance the elastic electron wave field samples mainly the region containing the outermost atoms. Off resonance, the elastic wave field is more deeply penetrating and is limited only by the Bragg reflections (primary extinction) and by the inelastic scattering. Consequently, electron scattering measurements of a crystal property under resonance incidence conditions should yield a relatively good approximation to the "surface" as opposed to the "bulk" value. This idea was applied to the determina-

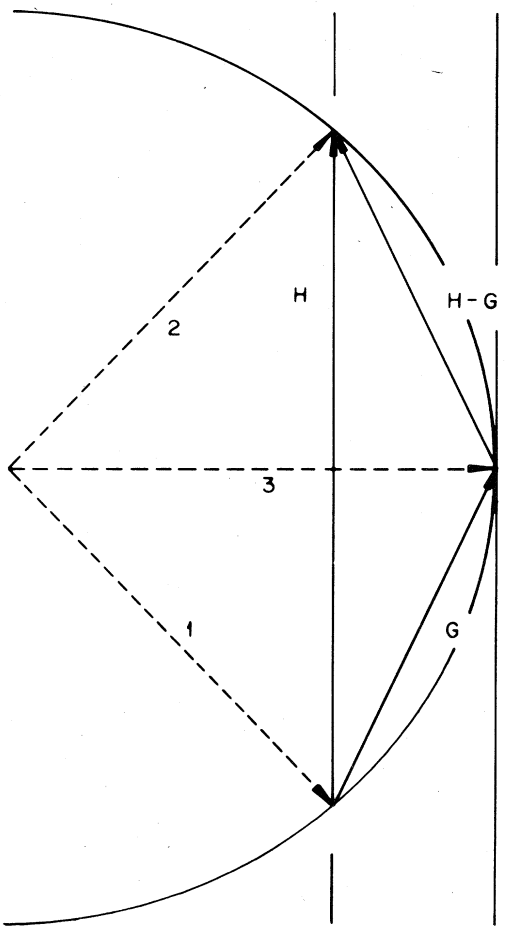

FIG. 18. Reciprocal space diagram illustrating the role of resonances in the temperature dependence of diffraction intensities. The circle denotes the Ewald sphere, broken arrows denote propagation vectors for (1) the incident beam, (2) the reflected beam, and (3) the intermediate or resonance beam. Vertical lines denote reciprocal-net rods. H, G, and H–G denote possible momentum transfers (see text, Sec. III.D).

tion of the sublattice magnetization of NiO(001) surface layers by LEED (Namikawa, 1978).

4. Spin polarization of reflected electrons

The spin polarization of electrons reflected by solids has the same origin as spin polarization in electron-atom scattering—namely the interaction between the electron spin and the magnetic field due to the orbital motion of the electron. For atoms the spin polarization increases rapidly with increasing atomic number and increasing scattering angle. For solids the spin polarization is broadly similar to that for the constituent atoms, but there are substantial differences attributable to interatomic multiple scattering.

On physical grounds one expects these differences to be largest for conditions close to that for a resonance. The differential cross section for electron-atom scattering is largest near the forward direction (small scattering angles) so that electron reflection by a solid will ordinarily involve relatively few back scattering (large-scattering-angle) events. On the other hand, resonance scattering involves on the average a relatively large number of back scattering events at substrate atoms as the electrons undergo multiple reflections between the substrate and the surface potential barrier. Polarizations due to individual back scattering events will contribute additively to the total spin polarization.

The correlation between spin polarization and resonances was investigated in calculations by Jennings and Jones (1978). They calculated the relative numbers $N\uparrow$ of electrons reflected with spin up and $N\downarrow$ reflected with spin down for low-energy unpolarized electrons incident on W(001) surface. The polarization difference $N\uparrow - N\downarrow$ was found to fluctuate rapidly with respect to energy at energies near a resonance simulated by their model. The results of the calculation have not been checked experimentally, but indications of a correlation of the type predicted are offered by experiments on Au(011) surface (Müller, 1978).

5. Resonance fluctuation of inelastic reflection intensities

The overall process underlying any observation of inelastic reflection of electrons at surfaces is usually pictured as a sequence of events including an elastic reflection event. Thus in the simplest case of this picture there is (i) elastic reflection followed by inelastic scattering and (ii) inelastic scattering followed by elastic reflection. The obvious consequences of this simplest case are (i) the inelastic reflection intensity will exhibit resonance fluctuations with respect to varying incidence conditions at $(E, \mathbf{k}_{\parallel})$ values for elastic resonances and (ii) the inelastic reflection corresponding to excitation energy E' and parallel momentum transfer $\mathbf{k}'_{\parallel}$ will exhibit resonance fluctuations for $(E, \mathbf{k}_{\parallel})$ values displaced by $(E', \mathbf{k}'_{\parallel})$ from elastic resonances. The first of these effects has been observed as resonance enhancement of the electron energy loss spectrum of W(001) with and without adsorbed H (Ho, Willis, and Plummer, 1979; Willis, 1978).

In addition to elastic resonances, experiments such as electron energy loss spectroscopy should also detect resonances decaying by inelastic channels. The nature of these resonances is indicated by the relevant formulas resulting from Feshbach's theory [Eqs. (40)–(42) and following paragraph]. The resonance numerator will have appreciable values only for those excited states having sufficiently large overlap with the intermediate surface state. This means that decay channels corresponding to surface excitations (e.g., surface plasmons, surface vibrational excitations) as opposed to bulk excitations will be most likely to exhibit resonances. A possibility indicated by theory is that the probability of a surface excitation starting from the intermediate surface state is high enough for the resonance term to make a dominant contribution to the amplitude. In such a case the resonance would enhance the inelastic scattering intensity. Such resonance enhancement need not follow the selection rules for the direct transition and could have a weaker dependence on the parallel momentum transfer.

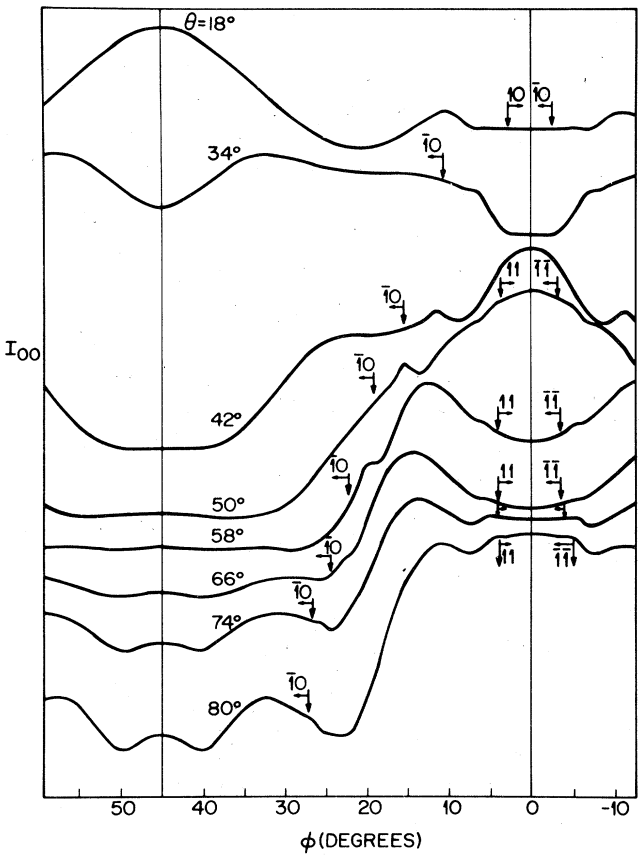

FIG. 19. Intensity data for Al(001) surface (Lauzier, 1971). The (00) beam intensity I_{00} is plotted versus azimuthal incidence angle ϕ for the indicated values of colatitude incidence angle θ and electron energy $E = 20.8$ eV. Vertical arrows indicate threshold conditions for the indicated beams. Horizontal arrows point to the side of the threshold to which the indicated beam is propagating.

IV. EXPERIMENTAL RESULTS AND COMMENTARY

A. Al(001)

1. Experiments

Measurements of the (00) LEED beam intensity as a function of the azimuthal angle of incidence ϕ were reported by Lauzier (1971) and by Lauzier, De Bersuder, and Hoffstein (1971). The measurements were made at a fixed electron energy of 20.8 eV for each of a series of values of colatitude angles of incidence θ ranging from 0° to 76° in steps of 2°. The LEED goniometer (Fig. 8) was used. Samples of the raw data (recorder tracings) are shown in Fig. 19.

2. Line shapes

Lauzier identified the weak and relatively narrow intensity fluctuations near the beam threshold positions (Fig. 19) as resonances. To locate the resonances as accurately as possible and to reveal their line shapes, he subtracted an arbitrarily smoothed background curve from each experimental curve. A representative line shape obtained in this way is shown in Fig. 20(a).

To simplify discussion, the line shape is here plotted against $e \equiv E - E_{\infty\bar{1}0}(k_{\parallel})$ rather than against ϕ as in the original presentation. While the procedure used to remove the background is a subjective one, it is definitely established that the line shape is asymmetric with a dip on the side far from the threshold, followed by a peak closer to the threshold.

The qualitative features of the line shape may be reproduced semiempirically using Eq. (61). The calculated line shape is shown in Fig. 20(b). The main physical assumptions underlying the calculation are of an image potential in the surface region and the "wide gap" assumption. To simulate the instrumental broadening in the experiment, the intensity $|T|^2$ calculated by Eq. (61) was convoluted with a Gaussian of width (FWHM) 0.5 eV. This is a typical value of incidence energy spread for the type of equipment used.

The calculated line shape [Fig. 20(b)] has two qualitative features whose presence does not depend on any special choice of parameters in Eq. (61). They are a long "tail" extending to the low-energy side, and a relatively narrow "blip" due to imperfectly resolved fine structure close to threshold. Neither of these features is present in the experimental line shape, Fig. 20(a). The absence of the tail might be an artifact of the background subtraction. Going back to the raw data, one can draw in another but equally plausible background curve that subtracted leaves a tail. While the threshold blip is not present in the cited experiments of Lauzier, there are other experiments on Al(001) (Henrich, 1975) that show a narrow feature located at the threshold (see Fig. 10). This narrow feature probably corresponds to the threshold blip in the theoretical curve, Fig. 20(b).

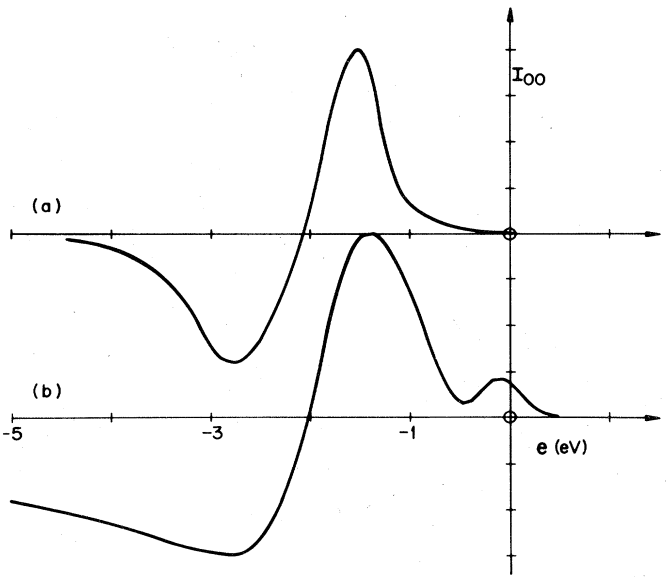

FIG. 20. (a) Representative lineshape of resonances observed at Al(001) surface (Lauzier, 1971). The lineshape shown was obtained by background subtraction from the plot of (00) beam intensity I_{00} versus azimuthal incidence angle ϕ for electron energy $E = 20.8$ and colatitude incidence angle 54°. e denotes the electron energy referred to the threshold energy of the $(\bar{1}0)$ beam. (b) Semiempirical fit to the observed line shape.

The parameter values used in Eq. (61) were chosen as follows:

$|T^0S| = 0.5$ (fit to energy separation of intensity extrema),

$\tau = 1.67$ (energy positions of extrema),

$\arg R = -0.47$ (ratio of positive and negative intensity excursions),

$|R| = 0.01$ (the observations apparently conform to the case of small resonance/direct ratios ($|R| \ll 1 - |T^0S|$) in which the line shape is insensitive to the value of $|R|$).

From the above value of $|T^0S|$ one infers, assuming $|S| = 1$, an intensity reflection coefficient of 0.25 for the intermediate wave involved in the resonance. The characteristic width of the resonance exclusive of instrumental broadening, as given by Eq. (63), is 1.8 eV. The value of τ yields through Eq. (62) a resonance binding energy $-e_1 = 1.9$ eV. Thus in this case the resonance position is close to the mean of the intensity extrema.

3. Surface resonance band structure

The part of the surface resonance band structure $E(\mathbf{k}_{\parallel})$ that can be obtained from available experimental data is shown in Fig. 21. The points plotted are the coordinates of $\mathbf{k}_{\parallel}$ for which the resonance energy $E(\mathbf{k}_{\parallel})$ is equal to the electron energy at which the measurements were done (20.8 eV). The $\mathbf{k}_{\parallel}$ values were calculated from an angular plot of resonance positions given by Lauzier. The conventions observed in making the conversions are those of Fig. 1. The formula used reads

$$\mathbf{K}_{\parallel} \equiv \mathbf{k}_{\parallel} + 2\pi\mathbf{g} = (2E)^{1/2} \sin\theta [\hat{\mathbf{a}}_1 \cos\phi + \hat{\mathbf{a}}_2 \sin\phi]. \quad (68)$$

The carets denote unit vectors. In the present instance γ in Fig. 1 is 90°. In accord with the interpretation of line shapes, the resonance energy was taken in every case to be the average of the intensity extrema.

The experimental points in Fig. 21 form series that are approximately parallel to branches of the free-electron band structure $E_{\infty g}(\mathbf{k}_{\parallel})$ labeled $\bar{1}0$, 10, and 11, respectively. Note that, according to Eq. (4), each branch $E_{\infty g}$ is circle centered at $-2\pi\mathbf{g}$. The points associated with the $\bar{1}0$ and 10 branches can be fitted approximately by the 2-D free-electron band structure $E(\mathbf{k}_{\parallel}) = E_{\infty g}(\mathbf{k}_{\parallel}) + e_1$ with a binding energy $-e_1$ pf 1.8 eV. The three points belonging to the 11 branch would require a binding energy of about 3 eV for fit. The results plotted in Fig. 21 show no indication of any interaction between resonance levels such as one might expect to observe especially near the crossings of free-electron branches.

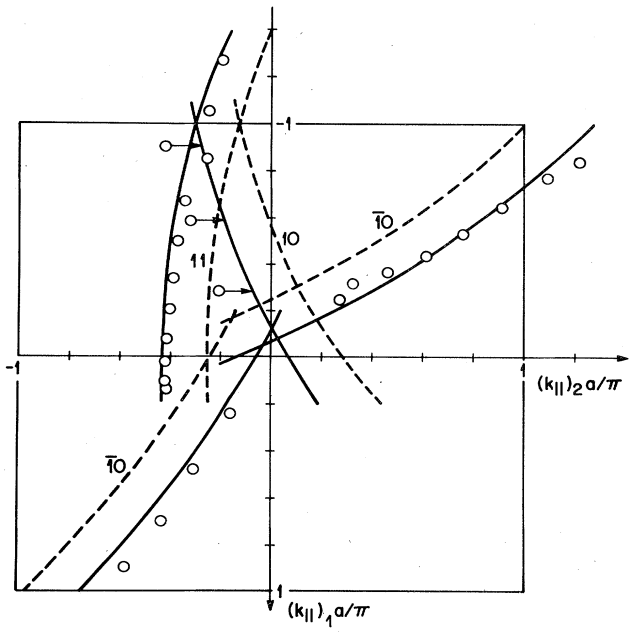

FIG. 21. Surface resonance band structure for Al(001). Open circles—experimental values (Lauzier 1971). Broken lines—branches of the free-electron band structure. Solid lines—branches of the 2-D free-electron band structure with binding energy 1.8 eV. $(k_{\parallel})_1$ and $(k_{\parallel})_2$ denote components of $\mathbf{k}_{\parallel}$ in the directions of the unit-mesh vectors $\mathbf{a}_1$ and $\mathbf{a}_2$, respectively (cf. Fig. 1). $a = 2.863$ Å is the unit mesh side for Al(001). The first surface Brillouin zone is outlined.

B. W(001)

1. Experiments

Measurements of the (00) LEED beam intensity as a function of energy were reported by Edwards and Propst (1972) (EP). The measurements were made at a fixed colatitude angle $\theta = 53°$ in the [01] azimuth ($\phi = 0$). The energy range was 0–40 eV. The apparatus used was a tandem of 127° electrostatic electron spectrometers providing electron energy resolution better than that of the conventional LEED experiment. The EP data showed narrow structure near 4 eV. This structure was interpreted by McRae (1971) as a resonance associated with the (01) beam threshold.

McRae and Wheatley (1972) (MW) reported conventional LEED measurements of the (00) beam intensity as a function of energy in the range 2–15 eV. The retarding field mode of LEED was used. The measurements were done at nominal θ values from 0° to 20° for two ϕ values, 0° and 45°. The incidence angle θ was not well determined in the MW experiments because the effect of the retarding field is to increase the angle by an unknown amount. Resonance structure was observed and correlated with that observed by EP. The assignment of the resonance to the (01) beam threshold was confirmed by these experiments.

Willis, Feuerbacher, and Christensen (1977) (WEC) observed resonances by the method of angle- and energy-resolved secondary electron emission. Measurements were reported for θ values from 0° to 70° on the $\phi = 0$ azimuth, and for emission energies from 0 to 30 eV. The resonances were observed as peaks lying inside the range of a forbidden gap [Fig. 12(b)].

High-resolution measurements of the (00) beam intensity spanning the energy range of the resonance were reported by Adnot and Carette (1977a) (AC). The apparatus used was a tandem of 127° spectrometers providing useful current density with energy resolution 15

meV and angle resolution better than 0.8°. The experiments were done for a fixed incidence direction ($\theta = 48°$, $\phi = 0$) but a range of 8° in θ was scanned by defocusing the primary beam and rotating the analyser. Willis (1978) (W) reported high-resolution experiments similar to those of AC but extending over a much wider range of colatitude angle of incidence θ. The range was $27° < \theta < 80°$.

2. Line shapes

The (00) beam intensity curves of EP and MW contain a peak about 1.5 eV wide centered near 3.5 eV, together with a narrower peak at higher energies. The curve of AC (Fig. 13) has an envelope similar to that found by EP and MW but the narrower peak observed in the earlier work was resolved by AC into a sequence of peaks starting with one at 4.75 eV. The peaks in this sequence become progressively narrower on going to higher energies.

The peak at 3.5 eV could be interpreted either as a very broad resonance of the "strong-overlap" type or as a Bragg peak. There is no easy way to distinguish between these two possibilities experimentally. The remaining structure starting with the peak at 4.75 eV is assigned to resonances of the "weak overlap" type. The peaks making up this sharper structure are numbered in order of energy starting arbitrarily with $n = 1$ for the 4.75 eV peak.

The qualitative features of the lineshape may be reproduced semiempirically using Eq. (61). In order to obtain a fit, it was necessary to adjust the value of the threshold energy $E_{\infty 01}$. The adjusted value used was 5.10 eV, about 0.15 eV higher than the (01) beam threshold energy for the θ value of the experiment. The origin of this upward displacement is not known but it might be simply the error in the determination of absolute electron energy in the AC experiment. The part of the AC intensity curve containing the resonance series is shown on an expanded energy scale in Fig. 22(a). The calculated curve is shown in Fig. 22(b). The intensities are plotted against $e = E - 5.10$ eV. In the calculated curve, instrumental broadening was simulated by convolution with a Gaussian of width 0.03 eV.

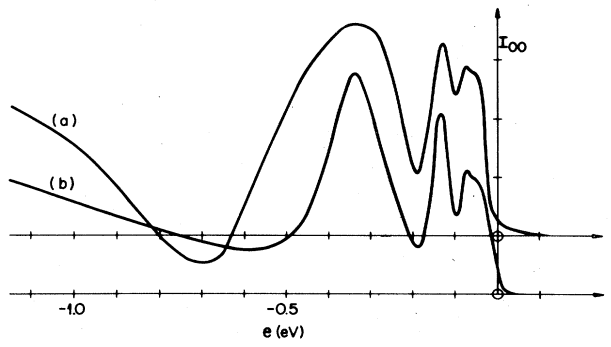

FIG. 22. (a) High-resolution intensity data for W(001) surface (Adnot and Carette, 1977a). The (00) beam intensity I_{00} is plotted as a function of energy e referred to an adjusted value of the (01) beam threshold (5.10 eV—see text, Sec. IV.B). (b) Semiempirical fit to the observed intensity curve.

The parameter values used in Eq. (61) were chosen as follows:

$|T^0S| = 0.3$ (fit to widths of two-highest-energy peaks),

$\tau = -0.1$ (energy positions of extrema),

$\arg R = -0.5$ (ratios of peak heights),

$|R| = 1.2$ (ratio of peak heights to background).

From the above value of $|T^0S|$ one infers (assuming $|S| = 1$) an intensity reflection coefficient of 0.1 for the intermediate wave involved in the resonance. The characteristic widths of the first four resonances exclusive of instrumental broadening, as given by Eq. (63) with $|T^0S| = 0.3$, are 0.34, 0.08, 0.03, and 0.01 eV, respectively. In fact, however, the width of the lowest-energy resonance peak in Fig. 22(a) is about twice that in the calculated curve [Fig. 22(b)]. The extra broadening is probably due to the overlap of the $n = 1$ resonance electron density distribution $|\psi_1(z)|^2$ with the crystal absorptive potential, resulting in a value of $|S|$ less than unity. As explained in Sec. III.C, this broadening effect ought to be particularly important for a small value of τ as apparently applies in the present instance.

The result that $|R|$ is of the same order as $1 - |T^0S|$ means that the resonance is intermediate between the limit of small resonance/direct ratios ($|R| \ll 1 - |T^0S|$) as represented by results for Al(001), and that of large resonance/direct ratios ($|R| \gg 1 - |T^0S|$) or enhancement commonly encountered in high-energy electron diffraction.

The value of τ yields through Eq. (62) an $n = 1$ resonance binding energy $-e_1 = 0.34$ eV. Thus in this case the $n = 1$ resonance position is close to that of the first intensity peak at −0.33 eV on the scale of Fig. 22.

That the fit requires a negative value of τ is an apparent anomaly that probably arises from the arbitrariness in numbering of resonances. Thus if the lowest sharp peak were assigned to $n = 2$ instead of $n = 1$, τ would be $2.0 - 0.1 = 1.9$. In fact a fairly good fit to the entire line shape (Fig. 13) may be obtained with renumbered levels and a slightly smaller value of τ, viz., $\tau = 1.6$. The $n = 1$ resonance binding energy in this case is $-e_1 = 1.73$ eV and the resonance positions are again close to those of the observed peaks.

In the secondary emission intensity curves of WFC, the resonance is observed as a peak about 1 eV wide. This peak is superposed on a rising background containing additional structure associated with variations of the bulk density of states [Fig. 12(b)]. The experiment was not capable of resolving higher-order resonances.

3. Surface resonance band structure

Experimental determinations are shown (Fig. 23) in comparison with the (01) and (00) beam thresholds and the positions of the edges of the forbidden gap. Also shown is a dispersion curve calculated by an LCAO method (Smith and Mattheiss, 1976).

The LEED experimental points (open symbols in Fig. 23) were calculated from experimental (00) beam intensity curves using Eq. (68). In accord with the interpretation of line shapes for the AC data, the resonance en-

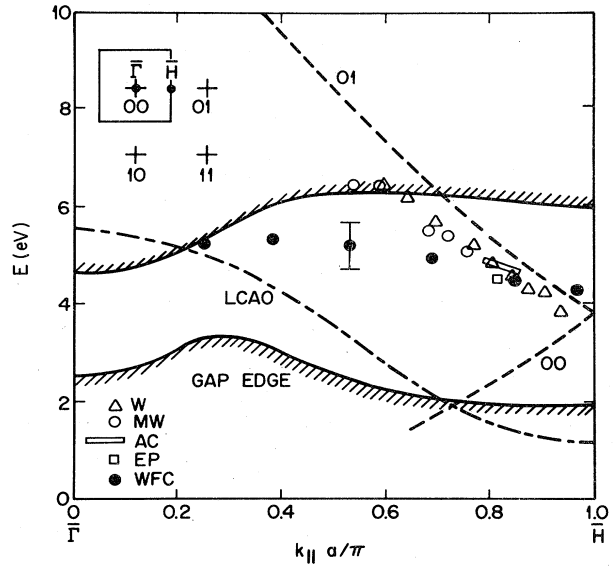

FIG. 23. Surface resonance band structure for W(001). Open symbols—values of $n=1$ resonance energies from LEED experiments. Filled circles—values from secondary emission experiments. Authors are identified in the text, Sec. IV.B. Broken lines—beam thresholds. Chain line—LCAO theory. Shaded lines—forbidden gap edges as given by WFC. $a=3.165$ Å is the unit mesh side for W(001). The first surface Brillouin zone is shown (inset, top left) with indications of symmetry points and reciprocal-net points.

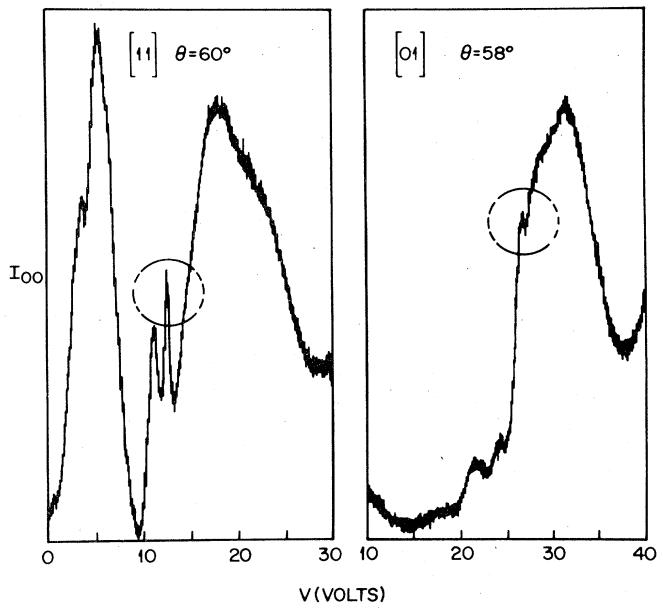

FIG. 24. Intensity data for Ni(001) surfaces (McRae, Aberdam, Baudoing, and Gauthier, 1978). The (00) beam intensity I_{00} is plotted versus accelerating potential for the colatitude angles θ and azimuth indicated. Circled features are identified as resonances.

ergies were taken in every case to be 0.2 eV higher than the energy at the maximum slope of the (00) intensity with respect to energy. This amounts to a slight revision of published estimates (McRae, 1978). The secondary emission experimental points (filled circles) are those obtained by WFC from their observed emission peak positions. The error bar is that published by WFC.

The LEED and secondary emission results do not agree with each other. The discrepancy might be due to error in locating the resonance center from the available secondary emission intensity curves. In these low-resolution results it is difficult to discriminate between resonance structure and structure associated with the bulk density of states.

The experimental dispersion curve represented in Fig. 23 by open symbols is close to the (01) threshold curve. The apparent binding energy varies from 0.9 to 0.3 eV with $k_{\parallel}a/\pi$ increasing from 0.6 to 0.9. This variation of apparent binding energy could be due to an increase in the bulk phase parameter τ on passing upwards through the band gap. This could cause an increase in binding energy on approaching the upper edge of the gap as observed (Fig. 23). The LCAO results apparently apply to the broader structure observed at lower energy, supporting an assignment of that structure to a resonance of the "strong overlap" type.

C. Ni(001) and oxygenated Ni(001)

1. Ni(001)

Measurements of the (00) LEED beam intensity as a function of electron energy were reported by McRae, Aberdam, Baudoing, and Gauthier (1978) (MABG). The measurements were made in the energy range 5–40 eV for colatitude angles θ ranging from 5° to 80° in both the [01] and [11] azimuths. The LEED goniometer (Fig. 8) was used. Samples of the raw data (recorder plots) are shown in Fig. 24.

MABG identified narrow features such as those cited in Fig. 24 as $n=1$ resonances. The positions of all fea-

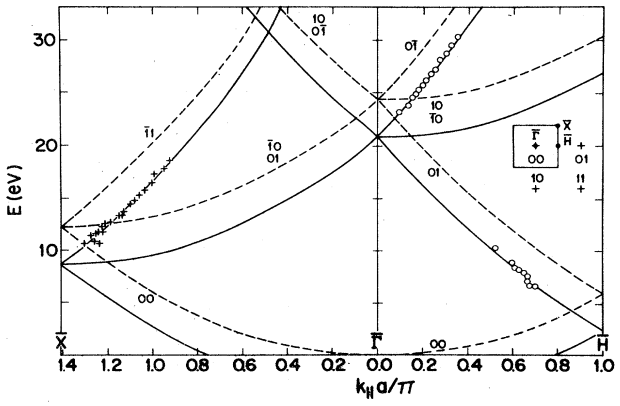

FIG. 25. Surface resonance band structure for Ni(001). Crosses and open circles—experimental values taken from observed (00) beam intensity maxima and minima, respectively. Broken lines—branches of the free-electron band structure. Solid lines—branches of the 2-D free-electron band structure with binding energy 3.5 eV. $a=2.492$ Å is the unit mesh side for Ni(001). The first surface Brillouin zone is shown (inset, right) with indications of symmetry points and reciprocal-net points. (McRae, Aberdam, Baudoing, and Gauthier, 1978).

tures with widths estimated to be less than 1.5 eV were plotted to determine the surface resonance band structure as shown in Fig. 25. As the resonances were very weak compared to the background it was not possible in this case to determine the resonance lineshapes. The positions plotted in Fig. 25 were of maxima or minima, whichever appeared the more prominent.

As illustrated in Fig. 25, the observed band structure is fitted accurately (± 0.3 eV) by the 2-D free-electron formula with a binding energy $-e_1 = 3.5$ eV. The value of binding energy is close to the maximum value for the image potential (3.4 eV). These data show no evidence of interaction between 2-D free-electron states. However, no resonances were observed in the vicinity of 2-D free-electron branch crossings, where a given interaction would produce the largest level displacements. Only a loose upper limit—0.5 eV—could be placed on the magnitudes of the interaction elements.

Net-current low-energy electron reflection measurements were reported by McRae and Caldwell (1978) (MC). The measurements were made in the energy range 0–30 eV for colatitude angles θ ranging from 0° to 8° in the [01] azimuth. This range of θ-values spans that omitted in the LEED experiment of MABG. The data were obtained in digital form, and narrow structure was accentuated by the use of a digital high pass filter as described by McRae, Landwehr, and Caldwell (1977) (MLC). In this technique the maximum width of the structure to be accentuated is selected by setting the passband cutoff frequency of the filter. The maximum width is roughly the reciprocal of the cutoff frequency. Representative examples of raw and filtered data are shown in Fig. 26. Figure 26(b) shows broad structure (width 3 eV) in roughly the positions expected for the (01) and (10, $\bar{1}$0) branches of the band structure shown in Fig. 25. In addition there is a narrower intensity fluctuation of which the peak (width 1 eV) is located exactly at the (10, $\bar{1}$0) threshold. This fluctuation is present in Fig. 26(b) but is shown against a flatter background in Fig. 26(c). It is probably the "threshold blip" due to imperfectly resolved fine structure that appears in calculated line shapes [cf. Fig. 20(b)]. Apparently the resonances observed by MABG are still present (though greatly broadened) near the center of the surface Brillouin zone.

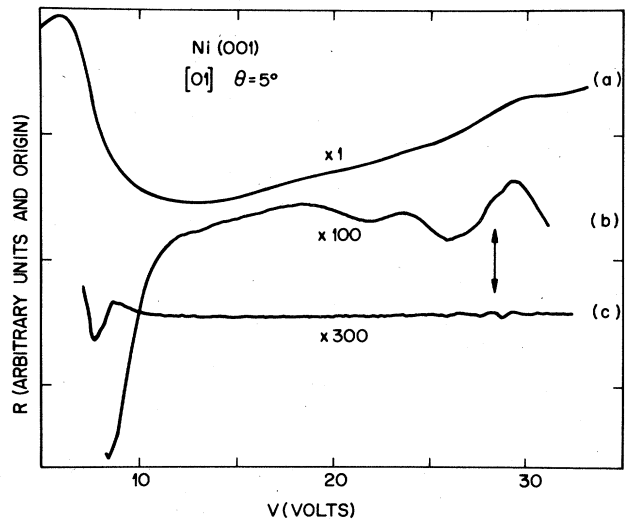

FIG. 26. Net-current data for Ni(001) surface (McRae and Caldwell, 1978). R denotes the negative of the net current, V the accelerating potential. Changes of R are directly proportional to changes of total reflection coefficient (secondary yield) with respect to variation of the accelerating potential. The data refer to the colatitude angle θ and azimuth indicated. The arrow marks the position of the (01) beam threshold. (a) Raw data, (b) filtered data, passband cutoff frequency 1/3.0 eV^{-1}, and (c) filtered data, passband cutoff frequency 1/0.96 eV^{-1}. Numbers alongside each curve indicate relative magnifications of the vertical scale.

2. Ni(001)$c(2 \times 2)$O

Net-current low-energy electron reflection measurements on oxygenated Ni(001) surfaces were made by MC and by MLC. The measurements were made in the energy range 0–30 eV for colatitude angles θ ranging from 0° to 16° in the [01] azimuth. The results were found to depend not only on the surface periodicty [$p(2 \times 2)$ or $c(2 \times 2)$] but also on the degree to which oxygen was incorporated in the bulk crystal. Figure 27 shows filtered

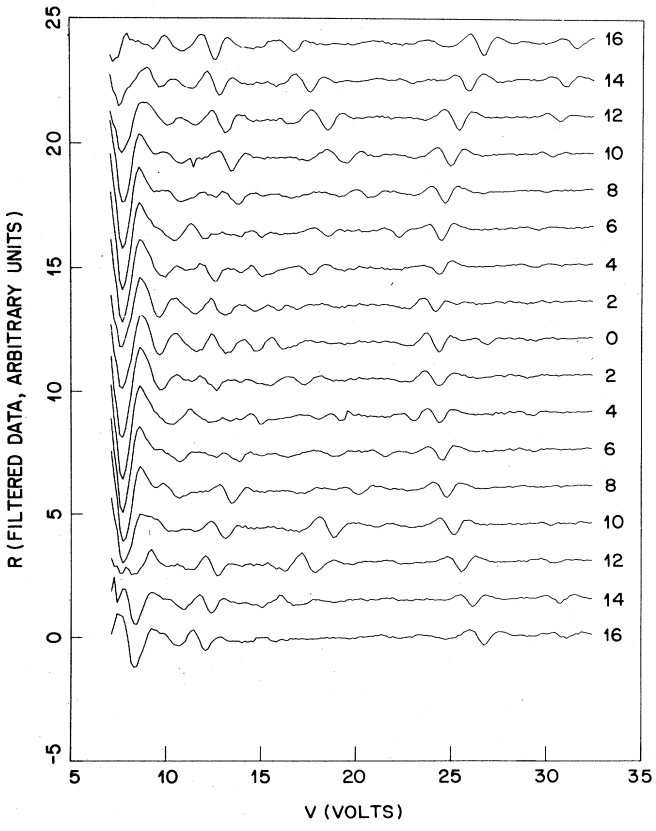

FIG. 27. Filtered net-current data (passband cutoff frequency 1/0.96 eV^{-1}) for Ni(001)$c(2 \times 2)$O surface (McRae, Landwehr, and Caldwell, 1977). R denotes the negative of the net current and V the accelerating potential. The numbers at right give values of the colatitude angle of incidence in degrees. The results refer to the [01] azimuth. Curves corresponding to both senses of rotation of the crystal are presented as a check of the normal incidence setting.

data reported by MLC for a Ni(001)$c(2\times2)$O surface prepared under conditions designed to minimize the bulk oxygen concentration. These results illustrate two commonly observed though imperfect regularities of resonance intensities: (i) Relatively large intensities are observed for a metal with an overlayer of adsorbed atoms compared with the pure metal, and (ii) Intensities increase with increasing values of colatitude incidence angle θ. Apparently, and not unexpectedly, the interactions driving resonances increase with increasing surface roughness and with decreasing surface-normal momentum transfer in the excitation step.

Figure 28 shows the surface resonance band structure obtained by mapping the positions of the minima in Fig. 27, together with a 2-D nearly-free-electron fit to the observed band structure. The interpretation given by MLC takes account of the relative intensities of the resonances. In Fig. 27 there is a series of pronounced features near 25 V and a parallel series of weaker features near 30 V. These series were assigned respectively to allowed and forbidden resonances associated with the doubly degenerate (10) and ($\bar{1}$0) thresholds. In accordance with the discussion leading to Eq. (49), the

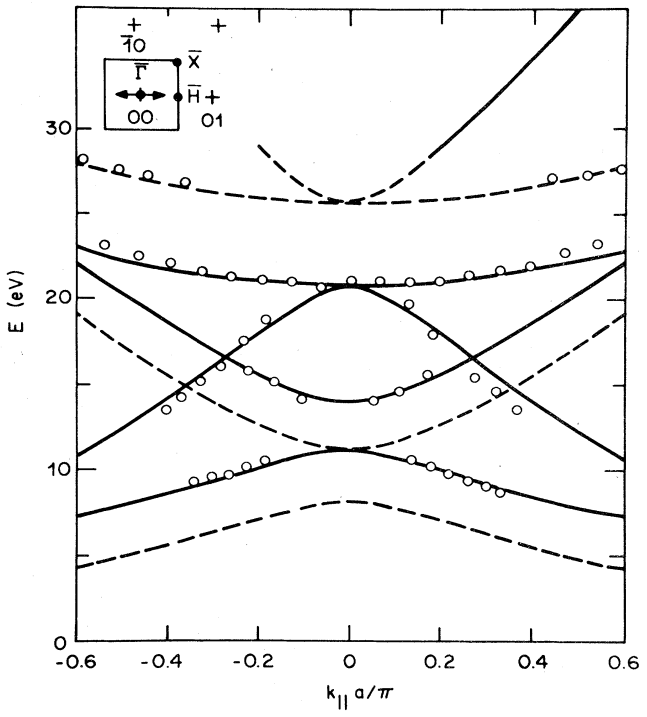

FIG. 28. Surface resonance band structure for Ni(001)$c(2\times2)$O surface. Open circles—experimental values taken from minima in filtered net-current curves. Lines denote branches of the surface resonance band structure calculated by the 2-D nearly-free-electron scheme with parameters adjusted to fit the data. Full and broken lines denote "allowed" and "forbidden" resonances, respectively. The partly broken line denotes a resonance forbidden at symmetry point $\bar{\Gamma}$. a = 2.492 Å is the unit mesh side for Ni(001). The first surface Brillouin zone is shown (inset, top left) with indications of symmetry points and reciprocal-net points. The arrows indicate the range of $k_{||}$ spanned by the main figure (McRae, Landwehr, and Caldwell, 1977).

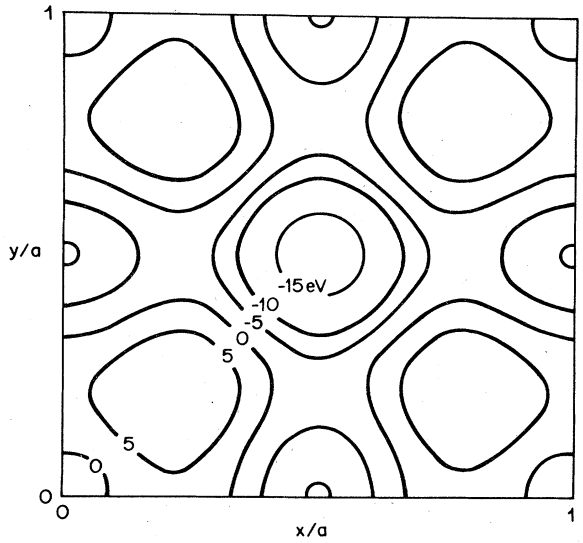

FIG. 29. Surface-weighted pseudopotential for Ni(001)$c(2\times2)$O surface. The potential is presented as a contour plot extending over one Ni(001) unit mesh of side a.

interaction element responsible for the splitting was found to have a negative sign and a value half that of the splitting, giving $\langle U_{20}\rangle = -2.5$ eV. The positions of the resonances gave the binding energy $-e_1 = 1.0$ eV. The one other nonzero interaction element required to fit the observed band structure with due attention to the intensities was $\langle U_{10}\rangle = 1.5$ eV. The error in each of these determinations was ± 0.2 eV.

The results shown in Fig. 28 demonstrate abilities to determine the surface resonance band structure and to fit it semiempirically by a method incorporating parameters describing the surface structure. These abilities amount to a means of surface structure determination.

In the case illustrated (Fig. 28) the structural parameters are Fourier coefficients of the surface-weighted pseudopotential. The surface-weighted pseudopotential synthesized from Fourier coefficients by Eq. (65) is shown in Fig. 29. As the angular range of the experiment did not extend far enough to permit a determination of the coefficients $\langle U_{1/2\,1/2}\rangle$, the results shown in Fig. 29 must be interpreted as an average over the four Ni(001) unit meshes in one $c(2\times2)$ unit mesh. The main features of the potential plot in Fig. 29 are a central region of negative potential and four regions of positive potential on the unit-mesh diagonals. These features are consistent with what is known about the structure of the Ni(001)$c(2\times2)$O surface from LEED intensity analysis (Demuth, Jepsen, and Marcus, 1973). The central negative (electron-attracting) region in Fig. 29 may be attributed plausibly to an adsorbed O atom located above the center of the square formed by four adjacent Ni atoms. The four positive regions may be attributed to diagonally directed Ni–O bonds.

D. Prospects for surface characterization

The developments surveyed in this article belong mainly to an exploratory stage in which the emphasis

has been on phenomena and physical mechanisms of resonances. The observations have been made in the course of experiments designed for other purposes. Beyond this exploratory stage there are prospects of using the observation of resonances as a means of characterizing surfaces. These prospects depend first on the properties of resonances as they are now understood in broad outline, and second on the existence of experimental and theoretical techniques that can be applied specifically to resonances.

1. Properties of resonances

The properties that bear on surface characterization may be summarized as follows.

Widespread occurrence

Low-energy electronic surface resonances are observed for all types of crystals (metal, insulator, and semiconductors) at energies up to at least about 50 eV and over a substantial fraction of the surface Brillouin zone.

Identification

Resonance features in electron scattering intensity plots are characteristically of small width in energy. Most features of width less than about 1.5 eV can be confidently assigned to resonances. Ancillary criteria include correlations with beam thresholds and with forbidden gaps.

Band structure

The electronic surface resonance band structure can be measured by electron scattering methods that are simple and widely available, e.g., LEED. It has been shown that the surface resonance band structure from observations of narrow resonances is well described by 2-D nearly-free-electron formulas. The ability to determine lateral surface structure by a fit to the surface resonance band structure using elementary theory has been demonstrated. It is feasible to test 3-D models of the effective potential at the surface by full-scale computations of the surface resonance band structure and comparison with experiment.

Line shapes

Fine structure of resonance profiles may be observed in high-resolution experiments. It is feasible to test models of the effective potential outside the outermost atom layer of the crystal by calculations of the line shape and comparison with experiment.

Relation to electron spectroscopies

Resonances may be observed as final states of electronic transitions as in photoemission spectroscopy or through resonance enhancement of inelastic scattering intensities as in electron energy loss spectroscopy.

Surface selectivity

Resonance experiments sample the spatial region lying largely outside the bulk crystal. This high degree of surface selectivity depends on the use of a high-pass filter or other means to accentuate narrow structure as opposed to broader "background" structure in electron scattering intensity curves. Resonances or other electronic states whose electron density distribution lies largely inside the bulk crystal are broadened by inelastic electron-electron collisions and so are not observed as narrow structure. Resonance experiments employing an effective means of background removal are more highly surface-selective than other electron scattering methods of surface characterization.

Simplicity of interpretation

Resonance observations are inherently simpler to interpret than other comparable types of observation. First, only one electronic state of the crystal is involved, not two as in photoemission spectroscopy or other electron spectroscopies. Second, the structure sensitive quantities are energy levels, not intensities as in conventional LEED.

2. Experimental and theoretical methods

The usefulness of resonance observations is limited by difficulties in locating resonance centers from measured intensity profiles and in resolving the finer details of these profiles. However, there is a very good prospect of overcoming these difficulties by exploiting available experimental techniques to measure intensities with higher angular and energy resolution, and by applying available theory to the computation of resonance lineshapes.

Experimental

The resolution required is about 1° and 30 meV FWHM. This is similar to that of electron energy loss spectroscopy as applied to vibrational spectroscopy of surfaces, and in fact elastic reflection resonance observations can be made conveniently in conjunction with electron spectroscopy. However, the resonance experiment is essentially simpler than the spectroscopic one in that high resolution is needed for only excitation or decay channels, not both. For example, the ideal resonance reflection experiment is in principle the same as conventional LEED except for provision of an electron monochromator in place of the electron gun. In practice two other modifications of conventional LEED would be desirable. First, channel electron multiplier arrays or other means should be used to offset the reduced incident current. Second, since resonance intensities tend to increase with increasing colatitude incidence angles θ the setup should permit display of the specular beam for θ values going up to 90° (grazing incidence).

Theoretical

Current theoretical calculations of LEED intensities and of surface band structure contain all but one of the elements required to deal with resonances. The missing element is the long-range part of the potential. By including this element it would be possible to trace the progression from "strong overlap" to "weak overlap" cases. Theoretical calculations could also offer much

needed guidance to the connection between line shape, the surface resonance band structure and band structure of the substrate crystal. Finally the interplay between theoretical and experimental studies of resonance line shape might clarify the nature of the long-range interaction, including especially its dependence on electron velocity.

ACKNOWLEDGMENTS

The writer thanks P. E. Best, M. J. Cardillo, R. E. Dietz, P. J. Jennings, K. Kambe, J. B. Pendry, L. Sanche, M. Schlüter, R. F. Willis, and members of the Groupe d'Etude des Surfaces (Grenoble) for constructive suggestions or criticism and for supplying original material.

REFERENCES

Abramowitz, M., and I. Stegun, 1964, *Handbook of Mathematical Functions* (U.S. Dept. of Commerce, Washington, D. C.), formulas 13.1.33 (p. 505) and 13.5.7 (p. 508).
Adnot, A., and J. D. Carette, 1977a, Phys. Rev. Lett. **38**, 1084.
Adnot, A., and J. D. Carette, 1977b, Phys. Rev. B **16**, 4703.
Appelbaum, J. A., and D. R. Hamann, 1972, Phys. Rev. B **6**, 1122.
Andersson, S., 1970, Surf. Sci. **19**, 21.
Andersson, S., and B. Kasemo, 1971, Phys. Status Solidi A **4**, 373.
Artmann, K., 1947, Z. Phys. **124**, 80, 154.
Bachrach, R. Z., D. J. Chadi and A. Bianconi, 1978, Solid State Comm. **28**, 931.
Best, P. E., 1975, Phys. Rev. Lett. **34**, 674.
Best, P. E., 1979a, Phys. Rev. B **19**, 1054.
Best, P. E., 1979b (to be published).
Bisi, O., C. Calandra, and F. Manghi, 1977, Solid State Commun. **32**, 249, 255.
Cole, M., 1974, Rev. Mod. Phys. **46**, 451.
De Bersuder, L., 1968, C. R. Acad. Sci. B **266**, 1489.
De Bersuder, L., 1974, Rev. Sci. Instrum. **45**, 1569.
Demuth, J. E., D. W. Jepsen, and P. M. Marcus, 1973, Phys. Rev. Lett. **31**, 540.
Devonshire, A. F., 1936, Proc. R. Soc. London Ser. A **156**, 37.
Edwards, D., and F. M. Propst, 1972, J. Chem. Phys. **56**, 3184.
Esterman, I., and O. Stern, 1930, Z. Phys. **61**, 95.
Estrup, P. J., and E. G. McRae, 1971, Surf. Sci. **25**, 1.
Feder, R., and J. B. Pendry, 1979.
Feshbach, H., 1958, Ann. Phys. **5**, 357.
Frisch, R., and O. Stern, 1933, Z. Phys. **84**, 430.
Gersten, J. I., and E. G. McRae, 1972, Surf. Sci. **29**, 483.
Goodman, F. O., 1977, Crit. Rev. Solid State Mater. Sci. **7**, 33.
Harris, J., and R. O. Jones, 1974, J. Phys. C **7**, 3751.
Hayakawa, K., and S. Miyake, 1974, Acta Crystallogr. A **30**, 374.
Henrich, V. E., 1975, Surf. Sci. **49**, 675.
Herring, C., and M. H. Nichols, 1949, Rev. Mod. Phys. **21**, 185.
Hirabayashi, K., 1968, J. Phys. Soc. Jpn. **25**, 856.
Ho, W., R. F. Willis, and E. W. Plummer, 1979 (to be published).
Inkson, J. C., 1973, J. Phys. F **3**, 2143.
Jennings, P. J., 1978, Surf. Sci. **75**, L773.
Jennings, P. J., and R. O. Jones, 1978, Surf. Sci. **71**, 101.
Jennings, P. J., and M. N. Read, 1974, Surf. Sci. **41**, 113.
Jones, R. O., 1975, in *Surface Physics of Semiconductors and Phosphors*, edited by C. G. Scott and C. E. Reed (Academic, New York).
Kawamura, T., Y. Ohkawa, and S. Miyake, 1976, J. Phys. Soc. Jpn. **40**, 226.
Kikuchi, S., and S. Nakagawa, 1933, Sci. Pap. Inst. Phys. Chem. Res. Tokyo **21**, 256.
Kohra, K., K. Molière, S. Nakano, and M. Ariyama, 1962, J. Phys. Soc. Jpn. **17** Suppl. B-II, 82.
Landau, L. D., and E. M. Lifshitz, 1965, *Quantum Mechanics*, (Pergamon, Oxford) 2nd edition, Secs. 128, 129, 132.
Lang, N. D., and W. Kohn, 1970, Phys. Rev. B **1**, 4555.
Lang, N. D., and W. Kohn, 1971, Phys. Rev. B **3**, 1215.
Lang, N. D., and W. Kohn, 1973, Phys. Rev. B **7**, 3541.
Lauzier, J., 1971, Thèse 3ème Cycle, Université Scientifique et Médicale de Grenoble.
Lauzier, J., L. De Bersuder, and V. Hoffstein, 1971, Phys. Rev. Lett. **27**, 735.
Lennard-Jones, J. E., and A. F. Devonshire, 1936, Nature (London) **137**, 1069.
MacColl, L. A., 1939, Phys. Rev. **56**, 699.
McRae, E. G., 1971, Surf. Sci. **25**, 491.
McRae, E. G., 1975, Surf. Sci. **47**, 167.
McRae, E. G., 1978, Phys. Rev. B **17**, 907.
McRae, E. G., 1979, J. Vac. Sci. Technol. (to be published).
McRae, E. G., D. Aberdam, R. Baudoing, and Y. Gauthier, 1978, Surf. Sci. (to be published).
McRae, E. G., and C. W. Caldwell, 1964, Surf. Sci. **2**, 509.
McRae, E. G., and C. W. Caldwell, 1967, Surf. Sci. **7**, 41.
McRae, E. G., and C. W. Caldwell, 1976a, Surf. Sci. **57**, 63.
McRae, E. G., and C. W. Caldwell, 1976b, Surf. Sci. **57**, 77.
McRae, E. G., and C. W. Caldwell, 1978, Surf. Sci. **74**, 285.
McRae, E. G., and H. D. Hagstrum, 1976, in *Treatise on Solid-State Chemistry*, Volume 6A, edited by H. B. Hannay (Plenum, New York), Chap. 2 (see especially pp. 83–110).
McRae, E. G., J. M. Landwehr, and C. W. Caldwell, 1977, Phys. Rev. Lett. **38**, 1422.
McRae, E. G., and G. H. Wheatley, 1972, Surf. Sci. **29**, 342.
Miyake, S., and K. Hayakawa, 1970, Acta Crystallogr. A **26**, 60.
Miyake, S., and K. Hohra, and M. Takagi, 1954, Acta Crystallogr. **7**, 393.
Müller, N., 1978 (private communication).
Namikawa, K., 1978, J. Phys. Soc. Jpn. **44**, 165.
Newton, R. G., 1966, *Scattering Theory of Waves and Particles* (McGraw-Hill, New York).
Pendry, J. B., and P. M. Echenique, 1978, J. Phys. C **11**, 2065.
Pendry, J. B., 1974, *Low Energy Electron Diffraction* (Academic, New York).
Read, M. N., and P. J. Jennings, 1978, Surf. Sci. **74**, 54.
Rowe, J. E., E. Margaritondo, and S. B. Christman, 1977, Phys. Rev. B **16**, 1581.
Rundgren, J., and G. Malmström, 1977a, Phys. Rev. Lett. **38**, 836.
Rundgren, J., and G. Malmström, 1977b, J. Phys. C **10**, 4671.
Schlüter, M., and M. L. Cohen, 1978, Phys. Rev. B **17**, 716.
Smith, N. V., and L. F. Mattheiss, 1976, Phys. Rev. Lett. **37**, 1494.
Wada, H., A. Suzuki, and T. Ichinokawa, 1976, quoted by Kawamura, Ohkawa and Miyake (1976).
Willis, R. F., 1975, Phys. Rev. Lett. **34**, 670.
Willis, R. F., 1978, private communication.
Willis, R. F., B. Feuerbacher, and N. E. Christensen, 1977, Phys. Rev. Lett. **38**, 1087.
Willis, R. F., B. Feuerbacher, and B. Fitton, 1976, Solid State Commun. **18**, 185.
Wood, E. A., 1964, J. Appl. Phys. **35**, 1306.